Intestinal *Akkermansia muciniphila* predicts clinical response to PD-1 blockade in patients with advanced non-small-cell lung cancer

Lisa Derosa[1,2,3,4,35], Bertrand Routy[5,6,35], Andrew Maltez Thomas[7,8,35], Valerio Iebba[9], Gerard Zalcman[10], Sylvie Friard[11], Julien Mazieres[12], Clarisse Audigier-Valette[13], Denis Moro-Sibilot[14], François Goldwasser[15,16,17], Carolina Alves Costa Silva[1,2], Safae Terrisse[1], Melodie Bonvalet[1], Arnaud Scherpereel[18], Hervé Pegliasco[19], Corentin Richard[5,6], François Ghiringhelli[20,21,22], Arielle Elkrief[5,6], Antoine Desilets[5,6], Felix Blanc-Durand[1], Fabio Cumbo[7], Aitor Blanco[7], Romain Boidot[23], Sandy Chevrier[23], Romain Daillère[24], Guido Kroemer[1,15,25,26,27], Laurie Alla[28], Nicolas Pons[28], Emmanuelle Le Chatelier[28], Nathalie Galleron[28], Hugo Roume[28], Agathe Dubuisson[1], Nicole Bouchard[29], Meriem Messaoudene[5,6], Damien Drubay[30], Eric Deutsch[1,4,31,32], Fabrice Barlesi[1,2], David Planchard[1,2], Nicola Segata[7,8], Stéphanie Martinez[33], Laurence Zitvogel[1,3,4,34] ✉, Jean-Charles Soria[1] and Benjamin Besse[1,2,4]

Aside from PD-L1 expression, biomarkers of response to immune checkpoint inhibitors (ICIs) in non-small-cell lung cancer (NSCLC) are needed. In a previous retrospective analysis, we documented that fecal *Akkermansia muciniphila* (Akk) was associated with clinical benefit of ICI in patients with NSCLC or kidney cancer. In the current study, we performed shotgun-metagenomics-based microbiome profiling in a large cohort of patients with advanced NSCLC ($n = 338$) treated with first- or second-line ICIs to prospectively validate the predictive value of fecal Akk. Baseline stool Akk was associated with increased objective response rates and overall survival in multivariate analyses, independent of PD-L1 expression, antibiotics, and performance status. Intestinal Akk was accompanied by a richer commensalism, including *Eubacterium hallii* and *Bifidobacterium adolescentis*, and a more inflamed tumor microenvironment in a subset of patients. However, antibiotic use (20% of cases) coincided with a relative dominance of Akk above 4.8% accompanied with the genus *Clostridium*, both associated with resistance to ICI. Our study shows significant differences in relative abundance of Akk that may represent potential biomarkers to refine patient stratification in future studies.

The development of ICIs targeting the PD-1–PD-L1 interaction has transformed the therapeutic landscape of patients with advanced NSCLC[1–6]. Landmark trials performed on previously treated patients with advanced NSCLC demonstrated superior overall survival (OS) following PD-1–PD-L1 blockade treatment compared with standard chemotherapy[1–3]. Following randomized phase III trials on patients with previously untreated advanced NSCLC, ICIs were approved in the first-line setting, either as monotherapy for patients with tumor PD-L1 expression ≥ 50% on tumor cells or in combination with platinum-doublet chemotherapy irrespectively of PD-L1 expression[4–6]. However, only a minority (35%) of patients benefit from sustained response to ICI[7]. Most patients with NSCLC develop primary or secondary resistance or occasional rapid acceleration of the disease, called hyper-progression[8]. Therefore, an understanding of mechanisms of resistance to ICI to identify novel and robust biomarkers of resistance is urgently needed.

Primary resistance has been attributed to low tumor mutational burden and poor intrinsic antigenicity of tumor cells[9,10], defective antigen presentation[11], limited intratumoral lymphocyte infiltration related to T cell exhaustion[12], and metabolic immunosuppressive pathways[13,14]. High-dimensional omics technologies are currently being developed to decipher the main regulators of the "cancer immune set-point"—the threshold beyond which an effective immune response can occur in the tumor bearer[15].

Recent lines of evidence point to the biological significance of the composition of the gut microbiota in influencing peripheral immune tonus and effectiveness of ICIs in patients with cancer[16]. The human gut microbiome, composed of 1×10^{13} micro-organisms, modulates many host processes, including metabolism, inflammation, peristalsis, elimination of pathogens and xenobiotics, maturation of immune functions to maintain tolerance to microbial and food antigens, and maintenance of intestinal epithelial barrier fitness. More recently, the gut microbiome has unexpectedly been shown to influence the effectiveness of ICIs[17]. First, in preclinical models, experiments with germ-free or antibiotic (ATB)-treated mice revealed that the antitumor activity of ICIs requires the presence of gut microbial components[18]. Similarly, ATB treatment prior to ICI initiation drastically reduced the clinical benefit in several cohorts of patients across various cancer types (melanoma,

advanced NSCLC, renal cell carcinoma (RCC), and urothelial cancer)[17,19–21]. This observation was confirmed in prospective trials and large meta-analyses, suggesting that gut microbiota may be instrumental for the immunostimulatory mode of action of ICIs[16].

Supporting this contention, we and others reported that primary responses to anti-PD-1–PD-L1 antibodies in patients with epithelial tumors and melanoma could, at least in part, be attributed to the taxonomic composition of the gut microbial ecosystem[17,19,22]. A diverse microbiota and the presence of specific bacteria, such as Akk or the *Ruminococcus* or *Bifidobacterium* genera, were associated with improved clinical response to ICI, correlating with increased systemic immune tonus[17,19,22]. We previously reported the stool metagenomic profiling of 100 patients diagnosed with refractory NSCLC or RCC who were receiving second- or third-line anti-PD-1 antibodies, and we concluded that the prevalence of Akk was increased in patients presenting partial response or stable disease, compared to patients in progressive disease (61% versus 34%, respectively, $P = 0.007$)[17]. Akk was also over-represented in patients with progression-free survival (PFS) > 3 months in an analysis of a subgroup of 60 patients with NSCLC[17]. Another group performed 16S ribosomal RNA (rRNA) gene amplicon sequencing of feces from 37 patients with NSCLC patient, confirming that Akk was enriched in patients who responded to ICI treatment[23]. In patients treated with abiraterone acetate, an inhibitor of androgen biosynthesis approved to treat metastatic castration-resistant prostate cancer, intestinal Akk also correlated with therapeutic responses[24]. Intestinal prevalence of Akk has also been associated with low body mass index (BMI), fitness, and successful aging (as indicated by its presence in disease-free centenarians)[25]. In animal models, Akk supplementation reduces obesity[26] and its co-morbidities, palliates neurodegenerative disorders[27], and counteracts progeria[28]. However, there are some epidemiological associations between this bacterium and inflammation-related pathologies (such as Parkinson disease[29], colitis during graft-versus-host disease[30], or diet-induced susceptibility to pathogenic *Citrobacter rodentium*[31]). Despite these reports, Akk may be viewed as a potential master regulator of homeostasis in the metaorganism.

Altogether, our earlier results obtained in small cohorts overlooking confounding factors allow us to surmise that the gut microbiome composition, and more specifically the presence of Akk at diagnosis, could become a biomarker predicting objective responses and 12-month survival rates in advanced NSCLC treated with first- and second-line ICIs. To validate this hypothesis, we performed a prospective multicentric study and analyzed baseline microbiome profiles using two metagenomic taxonomic pipelines in 338 patients with advanced NSCLC to predict the clinical benefit to anti-PD-1 antibodies in multivariate analyses.

Results

Association between *A. muciniphila* and clinical outcome. From December 2015 to November 2019, a total of 493 patients were screened for enrollment in this study, and 338 met inclusion criteria. Participants provided at least one baseline (V1 and/or V2) fecal sample for profiling (Extended Data Fig. 1). Using shotgun metagenomic sequencing, we determined that Akk was detectable in 131 (39%) and absent in 207 (61%) patients, and we used MetaPhlAn profiling expanded to identify the main Akk species-level genome bin (SGB9226 spp.[32], Supplementary Table 1). Baseline characteristics were well balanced between patients with detectable Akk (Akk^+) and undetectable Akk (Akk^-) with respect to sex, Eastern Cooperative Oncology Group (ECOG) performance status, smoking history, tumor histology, BMI, PD-L1 expression, and line of therapy (Supplementary Table 2a). However, there was a non-statistically-significant trend for older age in the Akk^+ group (66 years versus 64 years, $P = 0.08$). A total of 69 patients (20%) received ATBs 60 days prior to ICI initiation, with similar frequencies ($P = 0.68$) and regimen in Akk^+ and Akk^- groups (Supplementary Table 2a). Among ATB classes, beta-lactams were the most commonly prescribed in both groups (Supplementary Table 2b, 80% in Akk^+ versus 64% in Akk^-, $P = 0.33$).

For the Akk^+ and Akk^- groups in our cohort, objective response rates (ORRs) were 28% and 18%, respectively (Fig. 1a, $P = 0.04$). Partial response (PR), stable disease (SD), and progressive disease (PD) rates were 28%, 28%, and 44%, respectively, for the Akk^+ group versus 18%, 31%, and 50% for the Akk^- group. When considering the subgroup of patients who received immunotherapy alone as front-line treatment (1L IO, $n = 86$), ORRs were 41% and 19% in the Akk^+ and Akk^- groups, respectively (Fig. 1b, $P = 0.016$). Of note, for the whole cohort of patients (irrespective of the line of treatment), the median OS (mOS) was 18.8 months for the Akk^+ group, compared with 15.4 months in the Akk^- group (hazard ratio (HR) = 0.72; 95% confidence interval (CI) = 0.73–1.62; $P = 0.03$, Fig. 1c and Supplementary Table 2a). The median OS of patients who received immunotherapy as second-line treatment and beyond (≥2L) was 18.8 months in the Akk^+ group compared with 13.4 months in the Akk^- group (HR = 0.70; 95% CI = 0.50–0.98; $P = 0.04$, Fig. 1d and Supplementary Table 2a). For the 1L IO patients, 59% of Akk^+ patients were still alive after 12 months (OS ≥ 12), while only 35% of Akk^- individuals were long-term survivors (Fig. 1e, $P = 0.04$). We draw the same conclusions when using the MetaOMineR pipeline[33] (Extended Data Fig. 2a,b, left).

To establish cause–effect relationships between the presence of Akk (and its ecosystem) and response to ICIs, we retrospectively performed a preclinical meta-analysis by gathering 29 experiments

Fig. 1 | Stool Akk is associated with ICI clinical benefit. a,**b**, Correlations between stool Akk and ORR in 1L + 2L ($n = 338$) (**a**) and 1L ($n = 86$) (**b**) patients. CR; complete response. PR; partial response. SD; stable disease. PD; progressive disease. Data were analyzed using Chi-square test. *P* values are two-sided, with no adjustments made for multiple comparisons. **c**,**d**, Kaplan–Meier curves and Cox regression analyses of OS of 1L + 2L ($n = 338$) (**c**) and 2L ($n = 243$) (**d**) patients, according to Akk status. Akk status was compared using the stratified log-rank test. *P* values are one-sided with no adjustment. m; months **e**, Difference of the intestinal prevalence of Akk between patients with OS < 12 months *v* versus OS ≥ 12 months in 1L immunotherapy (IO), analyzed using Chi-square test. *P* values are two-sided, with no adjustments made for multiple comparisons. **f**–**h**, RNA sequencing of tumor biopsies in a subgroup of 44 patients (17 non-metastatic and 27 metastatic, Supplementary Table 4). **f**, Principal component analysis (PCoA) of the differentially expressed genes according to intestinal prevalence of Akk, using the 395 immune-related gene selection of the Oncomine Immune Response Research Assay, indicating significant differences using a Mann–Whitney $P < 0.10$ through PERMANOVA test with Euclidian distance. **g**, Heatmap of the differentially expressed gene products after normalization (between Akk^+ and Akk^- patients), classified by category. **h**, Boxplot of selected gene expression values according to Akk groups: Akk^+ ($n = 22$) and Akk^- (n = 22) patients (Supplementary Table 4). Differences between groups were assessed with Mann–Whitney tests. C-X-C motif chemokine ligand 10 (CXCL10), C-X-C motif chemokine ligand 9 (CXCL9), guanylate binding protein 1 (GBP1), vascular cell adhesion protein 1 (VCAM1), C-C chemokine receptor type 5 (CCR5), granzyme H (GZMH). The middle line of the box represents the median. The lower and upper hinges correspond to the first and third quartiles (the 25th and 75th percentiles). The upper whisker extends from the hinge to the largest value no further than 1.5 × IQR from the hinge (where IQR is the interquartile range, or distance between the first and third quartiles). The lower whisker extends from the hinge to the smallest value at most 1.5 × IQR of the hinge. Data beyond the end of the whiskers are called "outlying" points and are plotted individually.

in which tumor growth kinetics were followed up in avatar mouse models[34]. These recipients were treated with ATBs and then received fecal microbial transplants (FMTs) from 26 patients with NSCLC (Supplementary Table 3). Next, mice were implanted with syngeneic orthotopic MCA-205 sarcomas (representative tumor model for sensitivity to anti-PD-1 antibodies, as previously described[17,35]) and were later subjected to PD-1 blockade (Extended Data Fig. 2c–e). As observed in our clinical cohort, resistance to therapy in mice was associated with the absence of detectable Akk in the FMT experiments (Extended Data Fig. 2c,d).

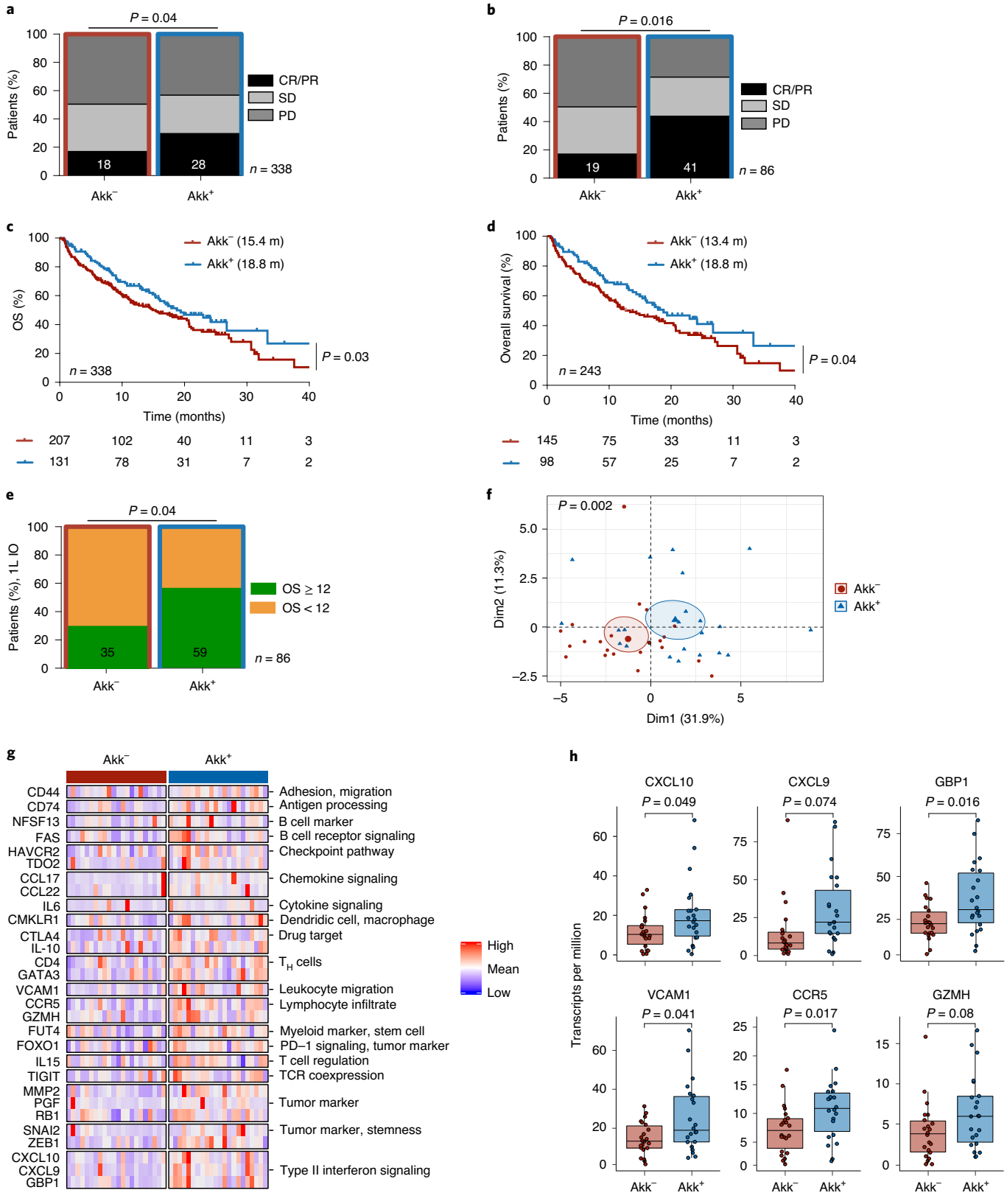

Therefore, in this second independent and prospective study on 338 patients with advanced NSCLC, we validated in humans using two different metagenomics pipelines, as well as in mice, that the presence of Akk is associated with higher ORR and longer OS in patients with NSCLC receiving ICIs.

***A. muciniphila*, the intestinal ecosystem, and the tumor microenvironment.** Given known correlations between compositional differences in the gut microbiota and tumor immune landscape[17,19] that can vary across histological types[36], we addressed the interactions between stool Akk detection and tumor histology (squamous versus non-squamous NSCLC). The presence of Akk in stools at diagnosis had no influence on histology (non-squamous versus squamous NSCLC; for multivariate analysis, $P = 0.556$ in Supplementary Table 2a).

In order to uncover intratumoral transcriptomic differences driven by Akk, we performed tumor RNA sequencing in a subset of patients with available tumor biopsies, which were collected from Akk$^+$ ($n = 22$) and Akk$^-$ ($n = 22$) patients upon diagnosis of locally advanced or metastatic NSCLC (Supplementary Table 4). The supervised analysis of significant gene expression differences between Akk$^+$ and Akk$^-$ groups within a panel of 395 immune-related genes of the Oncomine Immune Response Research Assay[37] revealed a set of differentially expressed genes associated with response to PD-1 blockade in lung cancer (Fig. 1f), such as CD4$^+$ T helper cells (T_H cells) with activation (*CD4*, *CD74*, *Vcam-1*, associated with adhesion and *trans*-migration of T lymphocytes within tumor nests[38]; granzyme H serine protease *Gzmh*, associated with cytolytic activity) and exhaustion (*Ctla4*, *Fas*, *Tigit*, *Havcr2*) markers and the IFN fingerprint (*Ccr5*, *Cxcl9*, *Cxcl10*, *Tdo2*, and IFN-inducible guanylate binding protein 1) (Fig. 1g,h). These results support the possibility that Akk could promote the elicitation or recirculation of T_H1 cells into the tumor microenvironment, as has previously been shown in mouse models[17,18].

Next, we examined compositional taxonomic differences in the gut microbiota in Akk$^+$ and Akk$^-$ patients. We found a significant increase of the Shannon diversity index (Extended Data Fig. 3a, top, $P < 0.0001$) in Akk$^+$ compared with Akk$^-$ patients, as well as differences in the overall microbial community composition (Extended Data Fig. 3a, bottom, $P = 0.0001$). Using LEfSe (linear discriminant analysis effect size) analyses to investigate differences in species relative abundance between the two groups, we found Ruminococcacae (*Ruminococcus bromii*, *Ruminococcus bicirculans*, *Ruminococcus lactaris*) and Lachnospiraceae (*Eubacterium siraeum*, *Eubacterium eligens*) family members and *Alistipes* spp. (*Alistipes inops*, *Alistipes finegoldii*, *Alistipes indistinctus*, *Alistipes shahii*) to be enriched in Akk$^+$ stools, as has previously been reported[39], whereas *Veillonella parvula*, *Actinomyces* spp., and genus *Clostridium* (*Clostridium innocuum, Hungatella hathewayi*) were overabundant in feces from Akk$^-$ patients (Extended Data Fig. 3b), as has already been described in the lower airway microbiome of patients with NSCLC with poor prognosis[40] as well as patients with kidney cancer resistant to ICIs[35].

Furthermore, within the Akk$^+$ group, we found significant differences in the overall microbial composition between patients with OS $\geq$ 12 months versus OS < 12 months, but this difference was not observed in Akk$^-$ patients (Fig. 2a, $P = 0.009$ versus $P = 0.07$). LEfSe analysis within the participants in the Akk$^+$ group with OS $\geq$ 12 months versus those with OS < 12 months unveiled an increased relative abundance of Lachnospiraceae family members (*Dorea formicigenerans*, *Dorea longicatena*, *Eubacterium rectale*, *Eubacterium hallii*, *Roseburia intestinalis*, *Coprococcus comes*) in patients with OS $\geq$ 12 months. Conversely, species belonging to the Gammaproteobacteria (*Escherichia coli*), the Clostridia class (*R. lactatiformans*), or the Bacilli class (such as *Lactobacillus gasseri, Lactobacillus paragasseri, Lactobacillus oris, Lactobacillus vaginalis*, *Streptococcus parasanguinis*) and *Veillonella parvula* were dominant in patients with OS < 12 months (Extended Data Fig. 3c).

Taken together, these results indicate that the presence of Akk is associated with important, potentially prognosis-relevant shifts in the intestinal microbiota and tumor microenvironment of patients with NSCLC.

Stratification of clinical outcome on the basis of the relative abundance of *A. muciniphila*. We unexpectedly found an over-representation of Akk in patients with OS < 12 months within the Akk$^+$ group, suggesting that the relative abundance of Akk may influence prognosis more than its absolute presence or absence. We next examined an ordinal, rather than a categorical (Akk$^+$ versus Akk$^-$), variable to analyze the clinical significance of Akk. Indeed, the relative abundance of Akk within the Akk$^+$ population ranged from 0.035% to 66.210%. Using a kernel density estimation of the relative abundance of Akk in patients with OS $\geq$ 12 or OS < 12 months, we noticed that patients harboring Akk^{high}, at a relative abundance greater than the 75th percentile (4.656%), did cluster within the OS < 12 months group (Fig. 2b,c, left, $P = 0.005$). To confirm this observation adjusting for other risk factors, we used a supervised approach to statistically define an optimal cutoff for Akk to discriminate two hypothetical groups of Akk$^+$ patients with different prognoses. We utilized a grid search algorithm, based on the multivariable Cox model (adjusted for age, sex, ECOG performance status, ATB exposure, histology, PD-L1, and line of treatment), with the Akaike information criterion as a performance index to determine the finest cutoff that corresponded to 4.799 (the 77th percentile of this cohort) (Fig. 2c, left). Among the whole cohort

Fig. 2 | Akk relative abundance represents a prognostic marker of ICI. a, Beta diversity measured by the Bray–Curtis Index, represented by PCoA, between Akk$^-$ versus Akk$^+$ groups and between OS < 12 months or $\geq$ 12 months within each subgroup. *P* values were calculated using PERMANOVA with 999 permutations. **b**, Kernel density estimation aligning two variables, OS < or $\geq$ 12 months and relative abundance of Akk (range: 0.035-66.210; 75th percentile: 4.656) in the entire cohort of 338 patients. The test used was the two-sided Fisher exact test on a 2 × 2 contingency table. No adjustments were required for this test. **c**, Distribution of the relative abundance of Akk in patients with detectable Akk (left) and percentages of patients within each of the three groups of Akk relative abundance (right). Akk$^-$, undetectable Akk; Akk^{low}, Akk relative abundance between 0.035-4.799%, Akk^{high}, >4.799% (77th percentile). The lower and upper hinges of boxplots correspond to the 25th and 75th percentiles, respectively. The midline is the median. The upper and lower whiskers extend from the hinges to the largest (or smallest) value no further than ×1.5 interquartile range from the hinge, defined as the distance between the 25th and 75th percentiles. **d**–**f**, Kaplan–Meier curve and Cox regression multivariate analysis of OS in 338 patients according to Akk relative abundance, segregated in 3 groups (Akk$^-$, Akk^{lo}, and Akk^{hi}) (**d**) and considering PD-L1 expression (**f**). Median OS of each group is indicated in round brackets. Akk status was compared using the stratified log-rank test. *P* values are one-sided with no adjustment. Cox logistic regression multivariate analysis of overall survival in 338 patients according to Akk relative abundance, segregated in 3 groups (Akk$^-$, Akk^{low}, and Akk^{high}) and all the other relevant clinical parameters (**e**). *P* values were calculated using the Wald test including all covariates in the Cox proportional hazards regression model. Exact *P* values are in Supplementary Table 6. m; months. **g**, Distribution (n (%)) of patients according to Akk relative abundance, segregated in two groups (Akk^{lo} and Akk^{hi}), and ATB use (no ATB, no exposure to ATB; ATB, exposure to ATBs within 2 months prior to ICI initiation). **h**, Kaplan–Meier curve and Cox regression multivariate analysis of OS in 338 patients segregated in 3 groups according to Akk relative abundance (Akk$^-$, Akk^{lo}, and Akk^{hi}) and ATB use (no ATB $n = 269$, left, and ATB $n = 69$, right). Akk status was compared using the stratified log-rank test. *P* values are one-sided with no adjustment. m; months.

of 338 patients, we observed that only 9% of patients (23% of Akk^{+} subgroup) fell into the category of "relative overabundance" of Akk (>4.799%), called Akk^{high} henceforth (Fig. 2c, right).

Moreover, we found a significant increase in Shannon diversity in specimens from Akk^{low} ("normal levels" of Akk in the gut) compared with Akk^{-} or Akk^{high} participants (Extended Data Fig. 4a,

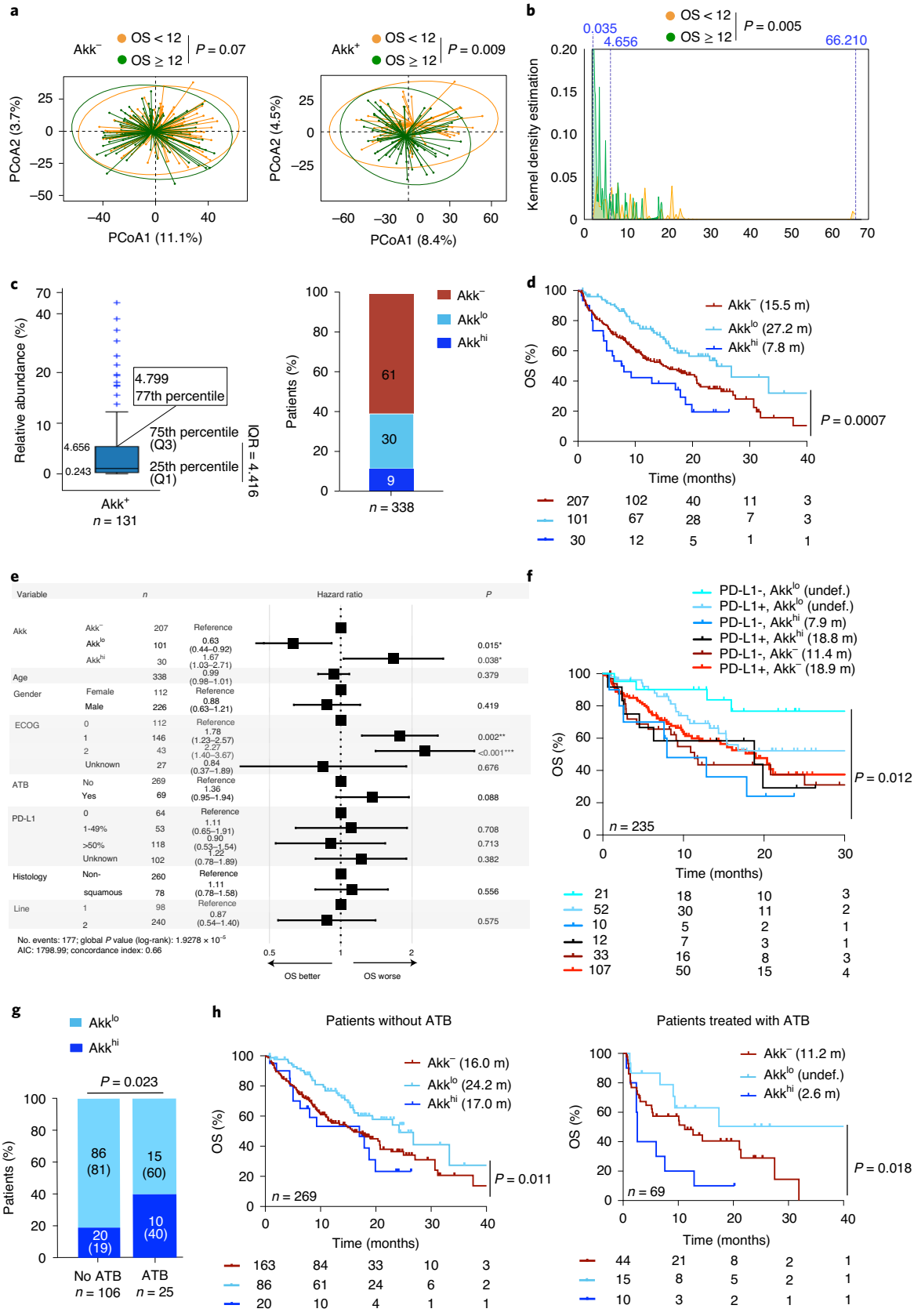

$P = 0.00003$), with the overall microbial community showing clear separation between Akk^{-} versus Akk^{low} as well as between Akk^{low} and Akk^{high} patients (Extended Data Fig. 4b,c, $P = 0.0001$ and $P = 0.0003$, respectively). Variable importance plot (VIP) discriminant analysis of taxonomic stool composition revealed that the ecosystem abnormally enriched in Akk (Akk^{high}) was over-represented by species of the genus *Clostridium* (*Clostridium symbosium*, *Clostridium innocuum*, *Clostridium scindens*, *Clostridium boltae*, *Clostridium clostridioforme*) at the expense of healthy commensals (*Faecalibacterium prausntzii, C. comes, E. rectale, D. formicigenerans, D. longicatena, Ruminococcus torques*, Extended Data Fig. 4d,e).

Kaplan–Meier survival curves, using the trichotomic stratification according to Akk relative abundance, diverged (log-rank test $P = 0.0007$, Fig. 2d and Supplementary Table 5a,b, with a significantly longer median OS for Akk^{lo} patients than for Akk^{hi} (27.2 months versus 7.8 months, Cox-adjusted HR = 0.38; 95% CI = 0.22–0.65, $P = 0.0005$) and Akk^{-} patients (27.2 months versus 15.5 months, adjusted HR = 0.63; 95% CI = 0.44–0.91, $P = 0.0150$). The HR for the other risk factors considered in the multivariate Cox regression analysis are presented in Fig. 2e and Supplementary Table 6. Not surprisingly, ECOG performance status ≥ 1 was another independent prognostic factor for this cohort[31]. The proportionality hazard assumption was questionable only for the ATBs (Schoenfeld residuals trend test, $P = 0.016$), but no statistically significant interaction with time could be identified. In addition, ATB exposure was associated with shorter OS in univariable analysis ($P = 0.009$; Supplementary Tables 5b and 6) and multivariate analysis ($P = 0.088$; Supplementary Table 6).

We also analyzed the interaction between Akk and PD-L1 in 235 patients with advanced NSCLC with available data on tumor expression of tumor PD-L1 (Supplementary Table 2a and Extended Data Fig. 1). We split the cohort into six groups according to PD-L1 expression and Akk fecal detection. The multivariate Cox regression analysis indicated that Akk dictated NSCLC prognosis, more than PD-L1 did ($P = 0.012$ in 235 patients, Fig. 2f).

Overall, we conclude that a trichotomic stratification of patients into Akk^{-}, Akk^{low}, and Akk^{high} may be a more accurate independent prognostic factor of OS than the dichotomous (Akk^{-} versus Akk^{+}) division (likelihood ratio test of multivariable Cox models: $P = 0.0009$). Akk^{low} may be considered as a surrogate of host intestinal fitness. Akk overruled PD-L1 as a predictive biomarker of response to ICIs in patients with NSCLC.

The impact of ATB use on *A. muciniphila* relative abundance and survival outcome. Akk^{high} levels as well as ATB exposure were considered standalone variables associated with shorter OS in patients with NSCLC treated with ICIs. Given these observations, we first combined the dichotomous classification of patients with respect to Akk (Akk^{-} versus Akk^{+}) with history of prior ATB exposure to segregate patients into four groups. The Akk^{+} group without ATB exposure showed the strongest clinical benefit (median OS of 23.0 months) compared with the three other groups (Extended Data Fig. 5a). The next favorable prognostic group was Akk^{-} without ATB exposure, with a median OS of 16.0 months. In contrast, exposure to ATB showed the shortest OS (mOS around 9 months, Extended Data Fig. 5a, $P = 0.017$). Accordingly, ATB tended to reduce the alpha diversity of the Akk^{+} group (Extended Data Fig. 5b,c). Moreover, ATB exposure enriched the Akk^{+} group in Gammaproteobacteria (*E. coli*), Clostridia class (*Clostridium bolteae, Ruthenibacterium lactatiformens*), and H2S-producing bacteria (*Bilophila wadsworthia*) (Extended Data Fig. 5d), as has already been described[35], at the expense of health-associated bacteria (*Collinsella aerofaciens*, *D. longicatena*, *D. formicigenerans*, *Eubacterium* spp. *CAG 38*)[34,41] also over-represented in the Akk^{+} group without ATB exposure (Extended Data Fig. 5e).

In an attempt to establish an association between ATB treatment and the relative overabundance of Akk, we compared the percentages of patients with Akk^{hi} stools between the ATB-treated and ATB-free groups (Fig. 2g) and generated a Kaplan–Meier OS curve using the trichotomic classification (Akk^{-}, Akk^{low}, and Akk^{high}) in two subgroups according to ATB exposure before the first ICI administration (Fig. 2h). We found a drastic increase of the proportion of Akk^{high} patients among ATB users (40% versus 19%, $P = 0.023$, Fig. 2g). We confirmed that the overabundance of stool Akk at diagnosis in patients exposed to ATBs was associated with lower OS despite ICI therapy (Extended Data Fig. 5c and Fig. 2h, right). Among ATB-free participants, Akk^{high} patients exhibited reduced benefits from ICIs compared with Akk^{low} individuals, but their benefits were not worse than for the Akk^{-} subgroup (Fig. 2h, left).

Altogether, these results demonstrate that ATB exposure is a negative predictor of survival following ICI and is associated with overabundance of Akk (Akk^{hi}) and the relative dominance of *Clostridium* spp. (*C. bolteae*) and *Lachnoclostridium*.

Stratification of outcome on other components of *A. muciniphila*-associated ecosystem. We used various statistical methods, such as linear discriminant analysis effect size (Extended Data Fig. 3), volcano plot from analysis of variance (ANOVA) model (Fig. 3a), and the MaAsLin multivariate statistical framework (Supplementary Table 7), to compare taxonomic compositional variations between Akk^{+} versus Akk^{-} stools to identify 16 bacterial species, among which 14 were positively and 2 were negatively associated with Akk fecal prevalence independently of other confounding factors, such as age, gender, BMI, lines of therapy (Fig. 3a and Supplementary Table 7). Next, we performed Cox logistic regression multivariate analyses to determine the impact of each bacterium on patient clinical outcome using a trichotomic distribution of their respective relative abundances (according to the cutoff defined above). Apart from Akk, very few bacteria (except *Eubacterium hallii*, *B. adolescentis*, *Parasutterella excrementihominis*, *Intestinimonas butyriciproducens*, and *C. innocuum* already described to mediate immunomodulatory functions[43–45]) were also associated with prolonged (Fig. 3b,d) or reduced (Fig. 3f and Supplementary Table 7) survival following ICI therapy. These bacteria had a "linear dose–response" relationship, in contrast to what was observed for Akk. The presence of Akk along with *E. hallii* or *B. adolescentis* was found to accurately predict ORR and/or mOS in this cohort of 338 patients

Fig. 3 | Stratification of clinical outcome based on other components of the Akk-associated ecosystem. a, Volcano plot (indicating fold change (FC) and *P* values in MaAsLin2 statistical analyses) to segregate taxonomic species (with a prevalence > 2.5%) according to their relative abundance in baseline fecal specimen of 338 patients based on their association with Akk: species significantly associated with or excluded from Akk-enriched ecosystems (Akk^{+}, blue dots, Akk^{-}, red dots). *P* values were calculated testing the null hypothesis and using a two-sided test. **b**,**d**,**f**. Kaplan–Meier OS curves in 338 patients, according to the trichotomic distribution of the relative abundance of beneficial or harmful bacteria retained in the LEfSe model, MaAsLin2, and the Volcano plot/ANOVA (Supplementary Table 7. The trichotomic distribution was compared using the stratified log-rank test. *P* values are one-sided, with no adjustment. **c**,**e**,**g**, Influence of collateral bacteria associated with Akk (retained in Supplementary Table 7) in the Akk-associated impact on ORR and OS in a dichotomic pattern (presence/absence) using the Chi-square test (for ORR, left, *P* values are two-sided, with no adjustments made for multiple comparisons). Cox regression multivariate analysis for Kaplan–Meier curves (right). The trichotomic distribution was compared using the stratified log-rank test. *P* values are one-sided with no adjustment.

with NSCLC (Fig. 3c,e). Hence, these findings suggest that Akk and its collateral commensalism may participate in the clinical benefit mediated by ICI.

***A. muciniphila* rescued response to PD-1 blockade by shifting the microbiome.** To establish a link between Akk and/or its collateral ecosystem and patient clinical outcome, we turned to our

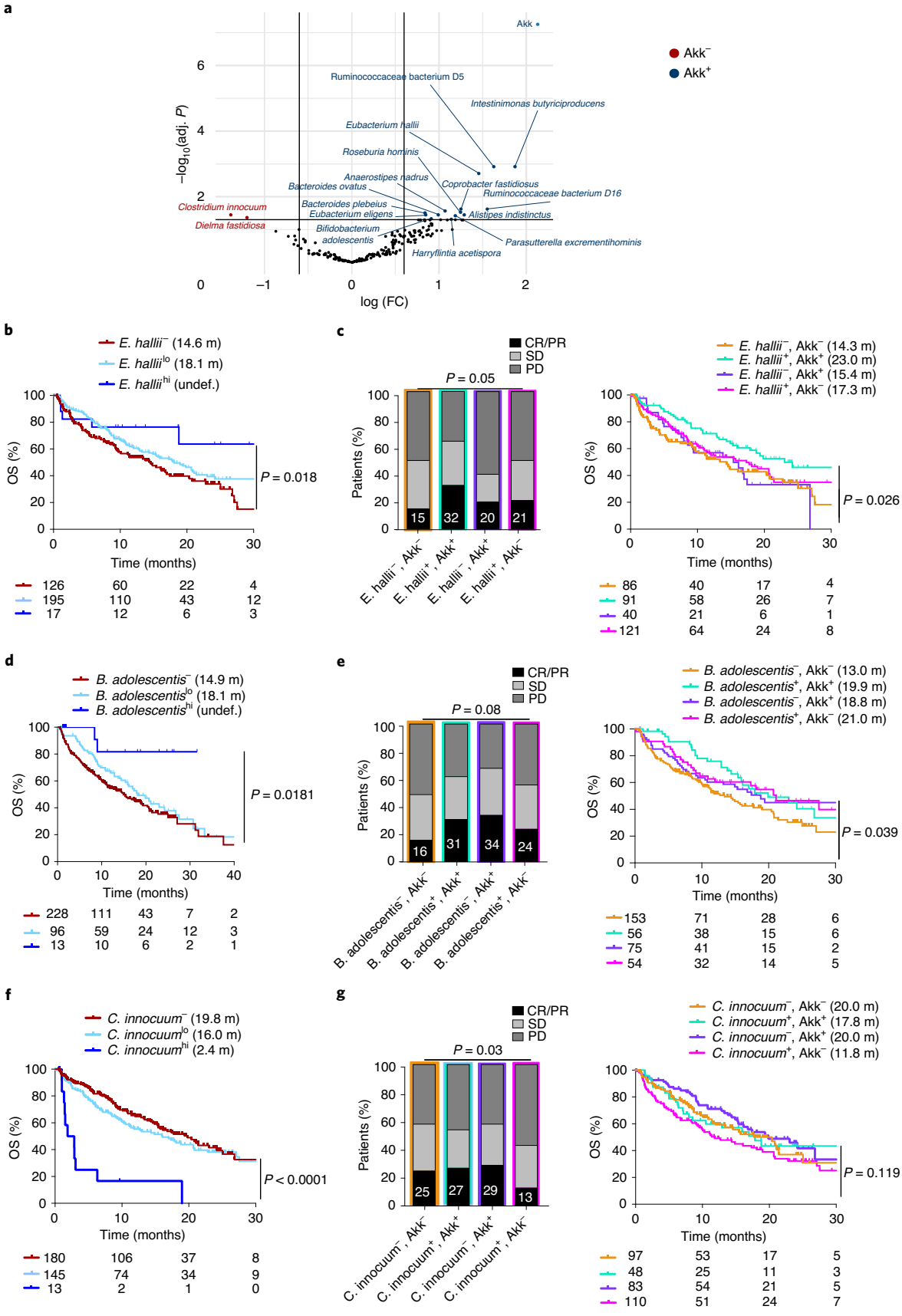

avatar tumor-bearing mouse models with humanized microbiota, described above. As depicted and commented on above (Extended Data Fig. 2c–e), mouse resistance to anti-PD-1 antibodies was associated with FMT bereft of Akk. Next, we analyzed the compensatory effects brought up by oral supplementation with an immunogenic strain of Akk, Akkp2261 (ref. [17]) in both groups of animals, recipients of Akk$^+$ or Akk$^-$ FMTs. Mice reared in specific pathogen-free conditions (SPF) (indicated as FMT– in Extended Data Fig. 6a,b) and inoculated with the same tumor cell line were used as controls of "murine eubiosis". Indeed, we could restore responsiveness to PD-1 blockade only in the setting of Akk$^-$ FMT (Extended Data Fig. 6b,c). Next, our objective was to analyze whether oral supplementation with Akkp2261 would change the host microbiome of the recipient mice and whether remodeling of the host ecosystem would correlate with preclinical benefit to exogenous Akkp2261. For this purpose, we concatenated all tumor models syngeneic of BALB/c (CT26, 4T1) and C57BL/6 (B16F10, MCA-205, MC38) mice that first received stools from 29 patients with NSCLC (Supplementary Table S3) and then were treated with anti-PD-1 antibodies (Extended Data Fig. 6a), and we next collected recipient feces before and after oral feeding with Akkp2261. The non-supervised hierarchical clustering of the ratios between the tumor growth kinetics with anti-PD-1 antibodies with or without exogenous Akkp2261 normalized on the effect of PD-1 blockade in eubiotic conditions (SPF versus FMT) revealed that exogenous Akkp2261 was effective in about 50% of cases (Extended Data Fig. 6d,e, left). We detected taxonomic differences in the recipient microbiota in responders (R) versus non responders (NR) to exogenous Akkp2261 (Extended Data Fig. 6e, right). Compared with NR mice, R mice harbored a relative over-representation of metagenomics species (namely *I. butyriciproducens* and *Parasuterrella excrementihominis*), annotated in Fig. 3a, in stools from humans harboring Akk$^+$. In contrast, NR mice tended to be enriched in *Bacteroides* spp. (Extended Data Fig. 6e, right).

Altogether, avatar mice that received Akk$^-$ human fecal material exhibited a phenotype of tumor resistance to PD-1 blockade but were rescued by *Akkp2261* when *Akkp2261* could shift the microbiome toward the favorable Akk-associated collateral ecosystem.

Discussion

Here, we report the results of a prospective, multicentric study based on the profiling of the gut microbiota of patients with advanced NSCLC treated with PD-1 blockade. The relative abundance of Akk was associated with clinical benefit, defined by an increase in ORR and survival, taking into accounting the main microbiota-relevant confounding factors (age, gender, BMI, lines of therapy). The prognostic significance of this gut bacterium was validated by multivariate analyses and interaction studies, which indicated that Akk is markedly associated with response of NSCLC to treatment with ICIs, independently of age, gender, ECOG performance status, ATB use, and PD-L1. The intestinal residence of Akk was a proxy for richness of the gut ecosystem, as shown by the association of Akk, at a relative abundance within the 77th percentile (Akk^{low}, <4.799%), with stool alpha diversity (Shannon diversity index). These results expand on previous observations that have been made in smaller cohorts of patients with NSCLC[17,39] and provide evidence that gut microbiome diversity and composition, specifically the relative abundance of Akk, offer relevant information to predict survival of patients with NSCLC amenable to ICIs.

Our study is the largest metagenomics prospective analysis that attempted to validate Akk as a new prognostic factor for patients treated with ICIs. Our study results met the pre-specified criterium of statistical significance, which was set as a 10% ORR increase between Akk$^-$ and Akk$^+$ patients when considering all (mostly 2L) 338 patients with NSCLC (from 18.2% to 28.2% in ORR, Fig. 1a). Moreover, we also observed a >10% ORR increase between Akk$^-$ and Akk$^+$ (from 19% to 41% ORR, Fig. 1b), with a mOS advantage in 1L patients (Fig. 1e). Moreover, our study linked the gut microbiota composition to the tumor microenvironmental landscape, highlighting increased transcription of gene products of adaptive immunity and the IFN fingerprint. Finally, we validated in mice that Akk$^-$ stools conferred resistance to PD-1 blockade.

In addition to prospectively validating the hypothesis in a larger and homogeneous cohort, we report that Akk was associated not only with increased alpha diversity but also with a distinct bacterial community associated with health or immunogenic status, represented by Ruminococcacae (*F. prausnitzii*, *R. lactaris*) and Lachnospiraceae (*D. formicigenerans*, *D. longicatena*, *E. rectale*, *E. hallii*, *Roseburia faecis*, *R. intestinalis*) family members, as well as *B. adolescentis*, *I. butyricyproducens*, and others. These findings reconcile the results across several works, geographical distributions, and sequencing technologies, as *Faecalibacterium*, *Ruminococcus*, and *Bifidobacterium* have previously been reported to be enriched in North American, Japanese, and South Korean patients with melanoma and NSCLC cancers who had favorable outcomes[19,34,39,42]. Moreover, even in avatar gut-humanized mouse models, the microbiomes of responders to exogenous Akkp2261 shifted toward an over-representation of some of the above mentioned species belonging to the Akk$^+$ ecosystem.

Confirming the clinical significance of bacterial diversity and commensals associated with responses, our results validate the growing body of evidence linking ATB use and poor clinical outcome[43]. In addition to depleting favorable genera associated with survival (such as Ruminococcus)[39], ATB use tends to deviate the gut microbiome composition toward harmful bacteria that have previously been associated with proinflammatory or immunoregulatory pathways (such as *E. coli* and *C. bolteae*)[44], supporting previous findings in renal cell carcinomas amenable to ICIs[35]. Surprisingly, in addition to acting as an independent negative prognostic factor, ATBs promoted an overabundance of Akk above the 77th percentile level, associated with poor prognosis. Indeed, ATB use doubled the proportion of individuals presenting a stool Akk^{high} phenotype. This phenotypic trait of overabundance of Akk >4.799% was associated with a dominance of the *Clostridium* species (*C. bolteae*, *C. innocuum*, *C. asparagiforme*, *C. scindens*, *C. symbosium*) belonging to clusters IV and XIVa of the genus *Clostridium*, known to maintain IL-10-producing regulatory T cells in colonic lamina propria[45].

Aside from ATB use, overabundance of Akk (>4.799%) was associated with a shorter OS than was a "normal" relative abundance of Akk (<4.799%), possibly reflecting an underlying pathophysiological disorder of the intestinal barrier in patients with advanced cancer. High relative proportions or subdominance of Akk in the ecosystem has been associated with pathophysiological failures (such as anorexia nervosa[46], GVHD[30], aging[47], dysmetabolism[48], HIV infection[49], pathobionts[50], and liver injury[51]). Hence, in the context of gut injury by, or conducive to, ATB use, Akk might constitute a biomarker of ongoing but imperfect intestinal repair. Of note, we failed to observe a similar trichotomic distribution correlating with opposite clinical outcome investigating other bacteria (Fig. 3).

Hence, we conclude that Akk's relative abundance could represent a reliable biomarker of favorable or dismal prognosis for patients receiving immunotherapy with PD-1 blockade. It may be of utmost importance to IO patients, risk-stratified on the basis of shot-gun metagenomics (rather than by 16S rRNA) sequencing, to precisely quantify the relative abundance of Akk in addition to ATB use and PD-L1 expression in patients with NSCLC in prospective trials designed to discover optimal biomarkers.

Therapeutic strategies modulating the microbiome, such as FMT or commensals, are currently being evaluated to boost ICI responses or circumvent primary resistance to ICI, though without patient stratification based on degree of dysbiosis[52]. Here we provide

preclinical data suggesting that Akk could therapeutically bypass the resistance to anti-PD-1 blockade conferred by FMT bereft of endogenous Akk (Extended Data Fig. 6 and refs. [17,34]). The oral supplementation with exogenous Akk (Akkp2261) was particularly effective when Akk shifted the recipient microbiome toward a healthy status (Extended Data Fig. 6d,e). A recent preclinical study indicates that the anticancer effects of recombinant interleukin-2 could be improved by Akk in a Toll-like receptor-2-dependent fashion[53]. In patients, food supplementation with Akk is safe and reduces insulin resistance and dyslipidemia in the context of pre-diabetes[48]. Altogether, we surmise that therapeutic supplementation with a lyophilized encapsulated Akkp2261 would benefit the subgroups of patients not exposed to ATB and devoid of endogenous Akk. In contrast, complex polymicrobial consortia or fecal microbial transplantation may be best suited for patients with prior ATB exposure.

The limitations of this study are the following. First, it did not evaluate the predictive value of Akk in 1L chemo-immunotherapy combinations (only considering 1L IO presenting with >50% PD-L1 tumor expression). Second, it could not consider the interactions between the tumor mutational burden and stool Akk prevalence. Moreover, this study failed to investigate the functional and clinical relevance of rarer *Akkermansia* spp.[54] different from the SGB9226 monitored in this study using MetaPhlAn 3 pipeline with a custom marker database (see Methods). Nevertheless, our study provides a strong rationale for the development of diagnostic tools for assessing gut dysbiosis for routine oncological management, as well as a framework for the design of microbiota-centered interventions to circumvent primary resistance to ICI in patients with NSCLC.

References

1. Herbst, R. S. et al. Pembrolizumab versus docetaxel for previously treated, PD-L1-positive, advanced non-small-cell lung cancer (KEYNOTE-010): a randomised controlled trial. *Lancet* **387**, 1540–1550 (2016).
2. Brahmer, J. et al. Nivolumab versus docetaxel in advanced squamous-cell non–small-cell lung cancer. *N. Engl. J. Med.* **373**, 123–135 (2015).
3. Borghaei, H. et al. Nivolumab versus docetaxel in advanced nonsquamous non–small-cell lung cancer. *N. Engl. J. Med.* **373**, 1627–1639 (2015).
4. Gandhi, L. et al. Pembrolizumab plus chemotherapy in metastatic non-small-cell lung cancer. *N. Engl. J. Med.* **378**, 2078–2092 (2018).
5. Paz-Ares, L. et al. Pembrolizumab plus chemotherapy for squamous non–small-cell lung cancer. *N. Engl. J. Med.* **379**, 2040–2051 (2018).
6. Reck, M. et al. Pembrolizumab versus chemotherapy for pd-l1–positive non–small-cell lung cancer. *N. Engl. J. Med.* **375**, 1823–1833 (2016).
7. Gadgeel, S. et al. Updated analysis from KEYNOTE-189: pembrolizumab or placebo plus pemetrexed and platinum for previously untreated metastatic nonsquamous non-small-cell lung cancer. *J. Clin. Oncol.* **38**, 1505–1517 (2020).
8. Ferrara, R. et al. Hyperprogressive disease in patients with advanced non-small cell lung cancer treated with PD-1/PD-L1 inhibitors or with single-agent chemotherapy. *JAMA Oncol.* **4**, 1543–1552 (2018).
9. Riaz, N. et al. Tumor and microenvironment evolution during immunotherapy with nivolumab. *Cell* **171**, 934–949.e16 (2017).
10. Rizvi, N. A. et al. Cancer immunology. Mutational landscape determines sensitivity to PD-1 blockade in non-small cell lung cancer. *Science* **348**, 124–128 (2015).
11. Spranger, S., Bao, R. & Gajewski, T. F. Melanoma-intrinsic β-catenin signalling prevents anti-tumour immunity. *Nature* **523**, 231–235 (2015).
12. Smyth, M. J., Ngiow, S. F., Ribas, A. & Teng, M. W. L. Combination cancer immunotherapies tailored to the tumour microenvironment. *Nat. Rev. Clin. Oncol.* **13**, 143–158 (2016).
13. Koyama, S. et al. Adaptive resistance to therapeutic PD-1 blockade is associated with upregulation of alternative immune checkpoints. *Nat. Commun.* **7**, 10501 (2016).
14. Young, A. et al. Co-inhibition of CD73 and A2AR adenosine signaling improves anti-tumor immune responses. *Cancer Cell* **30**, 391–403 (2016).
15. Chen, D. S. & Mellman, I. Elements of cancer immunity and the cancer–immune set point. *Nature* **541**, 321–330 (2017).
16. Derosa, L. et al. Microbiota-centered interventions: the next breakthrough in immuno-oncology? *Cancer Discov.* **11**, 2396–2412 (2021).
17. Routy, B. et al. Gut microbiome influences efficacy of PD-1-based immunotherapy against epithelial tumors. *Science* **359**, 91–97 (2018).
18. Vétizou, M. et al. Anticancer immunotherapy by CTLA-4 blockade relies on the gut microbiota. *Science* **350**, 1079–1084 (2015).
19. Gopalakrishnan, V. et al. Gut microbiome modulates response to anti-PD-1 immunotherapy in melanoma patients. *Science* **359**, 97–103 (2018).
20. Derosa, L. et al. Negative association of antibiotics on clinical activity of immune checkpoint inhibitors in patients with advanced renal cell and non-small-cell lung cancer. *Ann. Oncol.* **29**, 1437–1444 (2018).
21. Derosa, L. & Zitvogel, L. Antibiotics impair immunotherapy for urothelial cancer. *Nat. Rev. Urol.* **17**, 605–606 (2020).
22. Matson, V. et al. The commensal microbiome is associated with anti-PD-1 efficacy in metastatic melanoma patients. *Science* **359**, 104–108 (2018).
23. Jin, Y. et al. The diversity of gut microbiome is associated with favorable responses to anti-programmed death 1 immunotherapy in Chinese patients with NSCLC. *J. Thorac. Oncol.* **14**, 1378–1389 (2019).
24. Daisley, B. A. et al. Abiraterone acetate preferentially enriches for the gut commensal Akkermansia muciniphila in castrate-resistant prostate cancer patients. *Nat. Commun.* **11**, 4822 (2020).
25. Santoro, A. et al. Gut microbiota changes in the extreme decades of human life: a focus on centenarians. *Cell. Mol. Life Sci.* **75**, 129–148 (2018).
26. Zhou, Q. et al. Gut bacteria *Akkermansia* is associated with reduced risk of obesity: evidence from the American Gut Project. *Nutr. Metab.* **17**, 90 (2020).
27. Blacher, E. et al. Potential roles of gut microbiome and metabolites in modulating ALS in mice. *Nature* **572**, 474–480 (2019).
28. Bárcena, C. et al. Healthspan and lifespan extension by fecal microbiota transplantation into progeroid mice. *Nat. Med.* **25**, 1234–1242 (2019).
29. Romano, S. et al. Meta-analysis of the Parkinson's disease gut microbiome suggests alterations linked to intestinal inflammation. *NPJ Parkinsons Dis.* **7**, 1–13 (2021).
30. Shono, Y. et al. Increased GVHD-related mortality with broad-spectrum antibiotic use after allogeneic hematopoietic stem cell transplantation in human patients and mice. *Sci. Transl. Med.* **8**, 339ra71 (2016).
31. Desai, M. S. et al. A dietary fiber-deprived gut microbiota degrades the colonic mucus barrier and enhances pathogen susceptibility. *Cell* **167**, 1339–1353.e21 (2016).
32. Karcher, N. et al. Genomic diversity and ecology of human-associated *Akkermansia* species in the gut microbiome revealed by extensive metagenomic assembly. *Genome Biol.* **22**, 209 (2021).
33. Le Chatelier, E. et al. Richness of human gut microbiome correlates with metabolic markers. *Nature* **500**, 541–546 (2013).
34. Routy, B. et al. The gut microbiota influences anticancer immunosurveillance and general health. *Nat. Rev. Clin. Oncol.* **15**, 382–396 (2018).
35. Derosa, L. et al. Gut bacteria composition drives primary resistance to cancer immunotherapy in renal cell carcinoma patients. *Eur. Urol.* **78**, 195–206 (2020).
36. Meng, X. et al. Immune microenvironment differences between squamous and non-squamous non-small-cell lung cancer and their influence on the prognosis. *Clin. Lung Cancer* **20**, 48–58 (2019).
37. Hwang, S. et al. Immune gene signatures for predicting durable clinical benefit of anti-PD-1 immunotherapy in patients with non-small cell lung cancer. *Sci. Rep.* **10**, 643 (2020).
38. Nakajima, K. et al. IAP inhibitor, Embelin increases VCAM-1 levels on the endothelium, producing lymphocytic infiltration and antitumor immunity. *Oncoimmunology* **9**, 1838812 (2020).
39. Hakozaki, T. et al. The gut microbiome associates with immune checkpoint inhibition outcomes in patients with advanced non-small cell lung cancer. *Cancer Immunol. Res.* **8**, 1243–1250 (2020).
40. Tsay, J.-C. J. et al. Lower airway dysbiosis affects lung cancer progression. *Cancer Discov.* **11**, 293–307 (2020). https://doi.org/10.1158/2159-8290.CD-20-0263
41. Benevides, L. et al. New insights into the diversity of the genus *Faecalibacterium*. *Front. Microbiol.* **8**, 1790 (2017).
42. Lee, S.-H. et al. *Bifidobacterium bifidum* strains synergize with immune checkpoint inhibitors to reduce tumour burden in mice. *Nat. Microbiol.* **6**, 277–288 (2021).
43. Elkrief, A., Derosa, L., Kroemer, G., Zitvogel, L. & Routy, B. The negative impact of antibiotics on outcomes in cancer patients treated with immunotherapy: a new independent prognostic factor? *Ann. Oncol.* **30**, 1572–1579 (2019).

44. Seo, S. W., Kim, D., Szubin, R. & Palsson, B. O. Genome-wide reconstruction of OxyR and SoxRS Transcriptional regulatory networks under oxidative stress in *Escherichia coli* K-12 MG1655. *Cell Rep.* **12**, 1289–1299 (2015).
45. Atarashi, K. et al. Induction of colonic regulatory T cells by indigenous *Clostridium* species. *Science* **331**, 337–341 (2011).
46. Ruusunen, A., Rocks, T., Jacka, F. & Loughman, A. The gut microbiome in anorexia nervosa: relevance for nutritional rehabilitation. *Psychopharmacol.* **236**, 1545–1558 (2019).
47. van der Lugt, B. et al. *Akkermansia muciniphila* ameliorates the age-related decline in colonic mucus thickness and attenuates immune activation in accelerated aging Ercc1−/Δ7 mice. *Immun. Ageing* **16**, 6 (2019).
48. Depommier, C. et al. Supplementation with *Akkermansia muciniphila* in overweight and obese human volunteers: a proof-of-concept exploratory study. *Nat. Med.* **25**, 1096–1103 (2019).
49. Ouyang, J. et al. The bacterium *Akkermansia muciniphila*: a sentinel for gut permeability and its relevance to HIV-related inflammation. *Front. Immunol.* **11**, 645 (2020).
50. Huck, O. et al. *Akkermansia muciniphila* reduces *Porphyromonas gingivalis*-induced inflammation and periodontal bone destruction. *J. Clin. Periodontol.* **47**, 202–212 (2020).
51. Wu, W. et al. Protective effect of *Akkermansia muciniphila* against immune-mediated liver injury in a mouse model. *Front. Microbiol.* **8**, 1804 (2017).
52. Baruch, E. N. et al. Fecal microbiota transplant promotes response in immunotherapy-refractory melanoma patients. *Science* **371**, 602–609 (2020).
53. Shi, L. et al. Combining IL-2-based immunotherapy with commensal probiotics produces enhanced antitumor immune response and tumor clearance. *J. Immunother. Cancer* **8**, e000973 (2020).
54. Cani, P. D. & de Vos, W. M. Next-generation beneficial microbes: the case of *Akkermansia muciniphila*. *Front. Microbiol.* **8**, 1765 (2017).

[1]Gustave Roussy Cancer Campus, Villejuif, France. [2]Cancer Medicine Department, Gustave Roussy, Villejuif, France. [3]Institut National de la Santé Et de la Recherche Médicale (INSERM) U1015, Equipe Labellisée, Ligue Nationale contre le Cancer, Villejuif, France. [4]Université Paris-Saclay, Ile-de-France, France. [5]Department of Medicine, Centre Hospitalier de l'Université de Montréal (CHUM), Hematology-Oncology Division, Montréal, Quebec, Canada. [6]Centre de Recherche du CHUM (CRCHUM), Montréal, Quebec, Canada. [7]Department CIBIO, University of Trento, Trento, Italy. [8]European Institute of Oncology (IEO) IRCCS, Milan, Italy. [9]Department of Medical, Surgical and Health Sciences, University of Trieste, Trieste, Italy. [10]Thoracic Oncology Department-CIC1425/CLIP2 Paris-Nord, Hospital Bichat-Claude Bernard, AP-HP, Université Paris-Diderot, Paris, France. [11]Pneumology Department, Foch Hospital, Suresnes, France. [12]Department of Pneumology, Toulouse University Hospital, Toulouse, France. [13]Pneumology Department, Centre Hospitalier Toulon Sainte-Musse, Toulon, France. [14]Department of Thoracic Oncology, Centre Hospitalier Universitaire, Grenoble, France. [15]UPR 4466, Paris Descartes University, Sorbonne Paris Cité, Paris, France. [16]Department of Medical Oncology, Cochin Hospital, Assistance Publique-Hôpitaux de Paris, Paris, France. [17]Immunomodulatory Therapies Multidisciplinary Study Group (CERTIM), Paris, France. [18]Department of Pulmonary and Thoracic Oncology, University of Lille, University Hospital (CHU), Lille, France. [19]Pulmonary Department, European Hospital, Marseille, France. [20]Cancer Biology Transfer Platform, Centre Georges-François Leclerc, Dijon, France. [21]Centre de Recherche INSERM LNC-UMR1231, Dijon, France. [22]Department of Medical Oncology, Centre Georges-François Leclerc, Dijon, France. [23]Unit of Molecular Biology, Department of Biology and Pathology of Tumors, Georges-François Leclerc Cancer Center, UNICANCER, Dijon, France. [24]EverImmune, Gustave Roussy Cancer Campus, Villejuif, France. [25]Centre de Recherche des Cordeliers, INSERM U1138, Equipe labellisée—Ligue contre le cancer, Université de Paris, Institut Universitaire de France, Paris, France. [26]Metabolomics and Cell Biology Platforms, Institut Gustave Roussy, Villejuif, France. [27]Pôle de Biologie, Hôpital Européen Georges Pompidou, AP-HP, Paris, France. [28]Université Paris-Saclay, INRAE, MGP, Jouy en Josas, France. [29]Centre Hospitalier de Sherbrooke, Sherbrooke, Quebec, Canada. [30]INSERM U1018, Oncostat, Villejuif, France. [31]Department of Radiation Oncology, Gustave Roussy, Villejuif, France. [32]INSERM U1030, Radiothérapie Moléculaire et Innovation Thérapeutique, Villejuif, France. [33]Service des Maladies Respiratoires, Centre Hospitalier d'Aix-en-Provence, Aix-en-Provence, France. [34]Center of Clinical Investigations in Biotherapies of Cancer (BIOTHERIS) 1428, Villejuif, France. [35]These authors contributed equally: Lisa Derosa, Bertrand Routy, Andrew Maltez Thomas. ✉e-mail: laurence.zitvogel@gustaveroussy.fr

Methods

Study design and treatment. *Ethical issues.* The ancillary studies have been designed according to an IRB approved-study (Oncobiotics Sponsor Protocol N: Center for Security and Emerging Technology (CSET) 2017/2619, Agence nationale de sécurité du médicament et des produits de santé ID-RCB N: 2017-A02010-53, https://clinicaltrials.gov/ct2/show/NCT04567446). The trial was conducted in accordance with Good Clinical Practice guidelines and the provisions of the Declaration of Helsinki. All patients provided written informed consent. General Data Protection Regulation procedures and anonymization rules have been applied according to Oncobiome H2020 model system already in place in the ClinicoBiome, Gustave Roussy. All data and sample collection was performed in compliance with regulatory, ethical, and European GDPR requirements.

Patient eligibility. NCT04567446, a multicentric prospective observational study designed to evaluate the impact of the microbiome composition in the clinical outcome of patients with advanced NSCLC treated with anti-PD-L1–PD-L1. We enrolled across 12 academic centers in France and 2 in Canada. Adult patients with pathologically confirmed advanced non-squamous or squamous NSCLC and an ECOG performance status score of 0–2 who were amenable to ICIs as standard of care and who could provide a stool sample were eligible. Eligible patients received ICIs following progression on platinum-based chemotherapy regimens, either with nivolumab or atezolizumab regardless of PD-L1 expression or with pembrolizumab if PD-L1 was ≥1%. Given the subsequent approval of first-line ICI in the first-line setting during the study accrual period, patients who received pembrolizumab monotherapy or in combination with platinum-based chemotherapy, depending on PD-L1 expression, were also included. Standard-of-care treatment was continued until disease progression, unacceptable adverse effects, or completion as per the protocol (2 years of ICI treatment). Full eligibility criteria are listed in the trial protocol (NCT04567446). Baseline characteristics, including a detailed listing of concurrent medications received the 2 months prior to ICI initiation and the date of last follow-up, were entered at each center in an electronic case report form.

Hypothesis. Sample-size calculation was performed on the basis of the primary end-point, defined as investigator-assessed ORR from the hypothesis proposed in Routy et al.[17] that in a population with metagenomics detectable Akk (Akk^+) in the gut microbiome, the response rate would be higher than in the population with undetectable Akk (Akk^-). We considered that a meaningful clinical difference would correlate to an ORR incremental from 10% in the Akk^- to 20% in the Akk^+ group. Given the superiority hypothesis, power was set at 80% with a two-sided alpha level of 5%, using EAST program. Hence, we determined that at least 292 patients would be necessary to confirm our primary objective.

Study end-point and assessments. Computed tomography scans were performed at baseline and every 8–12 weeks for the first year and every 12–15 weeks thereafter until disease progression. Tumor response was assessed using the Response Evaluation Criteria in Solid Tumors version (RECIST) 1.1 (ref. [55]). The primary end-point was investigator-assessed ORR, which was defined as the number and percentage of patients with a best overall response (BOR) of confirmed complete response or PR. BOR was defined as the best response designation, recorded between the date of first treatment dose and the date of the initial objectively documented tumor progression per RECIST v1.1 or the date of subsequent therapy, whichever occurs first. For patients without documented progression or subsequent therapy, all available response designations contributed to the BOR determination. Secondary end-points included OS and microbiome variables, such as alpha and beta diversity and differential abundance analyses at the genus level. OS was defined as the time from trial inclusion until death from any cause. The follow-up of patients alive at the database lock was censored to the date of last record of contact.

Treatment modalities: the number of pembrolizumab (every other 21 days) or nivolumab (every other 15 days) or atezolizumab (every other 21 days) injections received was 4 ± 2 at 8–12 weeks and was 20 ± 4 at 12 months.

Human stool samples and metagenomics analyses. Fecal samples were prospectively collected (V1: pre-ICI, V2: before the second ICI injection, V3: at 3 months post-ICI, V4: at 6 months post-ICI) at each center following the International Human Microbiome Standards (IHMS) guidelines. Only the baseline V1 sample was considered for this analysis; for patients for whom such timely collection was not feasible, V2 samples were considered "baseline". For metagenomic analysis, the stools were processed for total DNA extraction and sequencing with Ion Proton technology following MetaGenoPolis (INRA) France, as previously reported[17,56,57]. Cleaning, filtering, and classification of reads were performed with two different pipelines: MetaOMineR and MetaPhlAn 3 (ref. [58]). In order to determine Akk presence or absence, we used a total of 463 genetic markers identified from 4 *Akkermansia* candidate species-level genome bins (SGBs) (SGB9223: 38 markers, SGB9224: 54 markers, SGB9226: 171 markers, SGB9228: 200 markers)[32] in MetaPhlAn. As outlined in Supplementary Table 1, the type of strain of *A. muciniphila* (MucT) delineated as SGB9226, was the most prevalent species in our cohort (>80% of *Akkermansia*-positive subset) and was therefore used for the calculation of the relative abundance of Akk in the main figures of this article.

We found msp_0025 to correspond to SGB9226, and used its relative abundance values as a proxy for *A. muciniphila* in MetaOMineR. A full description of both DNA purification and metagenomic pipelines is available in Derosa et al.[35]. Starting from abundance matrices, only taxa that were present in at least 2.5% of all samples were considered, and then raw data were normalized and standardized (SciKit-learn version 0.20.3).

Tumor RNA sequencing. Using a previously published technique[59], total RNA was extracted from formalin-fixed paraffin-embedded (FFPE) tumors from patients with advanced NSCLC included in the main analysis as well as from patients with limited stages (Supplementary Table 5). Libraries were prepared from 12 µl of total RNA with the TruSeq Stranded Total RNA using Ribo-Zero (Illumina) following manufacturer instructions. BBMAP v38.87 was used to trim the sequencing adapters and filtered the low quality and too short reads. Kallisto software[60] was used for quantifying transcript abundance from RNA-seq data against GRCh38 cDNA reference transcriptome from the Ensembl database, release 101. Only protein-coding transcripts and genes were included in the downstream analysis. Transcript Per Million values have been used for downstream analysis. Mann–Whitney tests have been performed to compare gene expression according to *Akkermansia* groups. PERMANOVA test with Euclidian distance has been used to assess the difference between groups on the subset of differentially expressed genes.

Preclinical study details. *Mice.* All animal experiments were carried out in compliance with French and European laws and regulations. The local institutional animal ethics board (Ministère de la Recherche, de l'Ènseignement Superieur er de l'Innovation) approved all mice experiments (permission numbers: 2016-049-4646, 2018-020-510263031v3). Mice avatar studies have been approved by the regulatory animal facility local and national committees (Ministère de la Recherche, de l'Ènseignement Superieur er de l'Innovation) (Everimmune no. 13366-2018020510263031 v3, APAFIS no. 17530-201811413352738 v2 (03/2019-03/2024). APAFIS no. 21378-201907080848483459). Female C57Bl/6 and BALB/c mice were purchased from Harlan and Janvier, respectively. Mice were used between 8 and 16 weeks of age and housed in SPF conditions. All mouse experiments were performed at the animal facility in Gustave Roussy Cancer Campus, where animals were housed in SPF conditions.

Cell culture, reagents, and tumor cell lines. MC38, MCA-205, B16F10 (syngeneic from C57BL/6 mice), and 4T1 cell lines (syngeneic from BALB/c mice) were purchased from ATCC. 4T1, MCA-205, and MC38 cells were cultured in RPMI 1640 containing 10% FCS, 2 mM L-glutamine, 100 UI/ml penicillin–streptomycin, 1 mM sodium pyruvate, and MEM non-essential amino acids. All reagents were purchased from Gibco-Invitrogen. B16F10 and CT26 cells were cultured in DMEM containing 10% FCS with 100 UI/ml penicillin–streptomycin and non-essential amino acids. All cell lines were cultured at 37 °C with 5% CO_2 and were regularly tested to confirm they were free of mycoplasma contamination.

Subcutaneous model of MCA-205, MC38, B16F10, and 4T1. Syngeneic C57BL/6 mice were implanted with 0.8×10^6 MCA-205, 1.0×10^6 MC38/CT26, or 3×10^5 B16F10 cells subcutaneously. Syngeneic BALB/c mice were implanted with 3×10^5 4T1 cells subcutaneously. For tumor growth experiments, tumor-implanted mice were treated intraperitoneally when tumors reached 20–40 mm^2 in size with anti-PD-1 monoclonal antibodies (250 µg/mouse; clone RMP1-14, lot 695318A1) or isotype control (clone 2A3, lot 686318F1). Mice were injected 4 times at 3-day intervals with anti-PD-1 monoclonal antibodies. Tumor length and width were routinely monitored three times per week using a caliper. All antibodies were purchased from BioXcell.

Antibiotic treatments. Mice were treated with an ATB solution containing ampicillin (1 mg/ml), streptomycin (5 mg/ml), and colistin (1 mg/ml) (Sigma-Aldrich) added in the drinking water of mice. Antibiotic activity was confirmed by cultivating fecal pellets resuspended in BHI + 15% glycerol at 0.1 g/ml on COS (Columbia Agar with 5% sheep blood) plates for 48 hours at 37 °C in aerobic and anaerobic conditions. In brief, in the context of fecal microbial transplantation experiments, mice received 3 days of ATB treatment before undergoing FMT the next day by oral gavage using animal feeding needles.

FMT experiments. FMT was performed by thawing fecal material. Two hundred µl of the suspension was then transferred by oral gavage into ATB pre-treated recipient (as described above). In addition, another 100 µl was applied on the fur of each animal. Two weeks after FMT, tumor cells were injected subcutaneously and mice were treated with anti-PD-1 monoclonal antibodies or isotype control, as previously explained. We used MCA-205 fibrosarcomas because, in SPF eubiotic mice, it is normally sensitive to anti-PD-1 antibodies and has been used as a reference mouse model in our previous avatar experiments reported in refs. [17,35]; both papers show that results obtained with MCA-205 were recapitulated in orthotopic TC1 lung cancer or RENCA models, respectively. So, we can trust the biological relevance and suitability of this MCA-205 model system to probe FMT or taxonomic fecal composition in future experiments.

Murine meta-analysis. We conducted 29 individual experiments over 2 years comprising 6–8 groups (including 6 mice per group). The growth kinetics of orthotopic MCA-205 sarcomas, and other tumors such as MC38 colon cancer (syngeneic from C57BL/6 mice), 4T1 breast or CT26 colon tumors (syngeneic from BALB/c mice), or B16 (melanoma), were monitored in avatar mouse models[34]. These recipients were ATB-treated and then received FMTs from 26 patients with NSCLC (phenotype of R versus NR to PD-1 blockade, and relative abundance of stool Akk, both described in Supplementary Table 6). Then, syngeneic tumors were implanted in mice, which were later subjected to immunotherapy with anti-PD-1 antibodies. FMT could confer sensitivity (when stools were Akk^{+}) or resistance (when stools were Akk^{-}) to anti-PD-1 antibodies, when compared with animals in eubiosis reared in SPF conditions (without FMT). Next, we analyzed the benefit and compensatory effects of oral supplementation of Akkp2261, based on presence or absence of Akk in the human donor's stool. Of note, exogenous Akkp2261 was not detectable more than 30 hours in the recipient intestines (as shown by qRT–PCR using *A. muciniphila*-specific probe sets). To better scrutinize whether the exogenous Akkp2261 could shift the microbiome of the recipient tumor-bearers differently in R versus NR mice, we concatanated all tumor models syngeneic of BALB/c mice (CT26, 4T1) and C57BL/6 mice (B16F10, MCA-205, MC38) that were treated by FMT from 29 patients with NSCLC and then treated the mice with anti-PD-1 monoclonal antibodies with or without Akkp2261 prior to stool collection for 16S-rRNA-based-sequencing of fecal amplicons. We calculated the relative benefit of exogenous Akk by dividing the ratio of (tumor size between anti-PD-1+ Akkp2261 /anti-PD-1+ water), normalized on the ratio of tumor sizes between anti-PD-1/control monoclonal antibodies in SPF mice for each time points for the whole kinetics. The non-supervised hierarchical clustering of the ratios between tumor growth kinetics with anti-PD-1 monoclonal antibodies with or without exogenous Akkp2261 normalized on the effect of PD-1 blockade in eubiotic conditions revealed that exogenous Akkp2261 was effective in about 50% cases (heatmap in Extended Data Fig. 3e). To delineate which Akk-associated ecosystem was associated with responses (ratios > mean of the cohort), LEfSe was used to identify the taxonomic changes segregating R versus NR to exogenous Akk. These species were compared with the bacteria in human stools described in Extended Data Fig. 1 and Fig. 3a.

Akk CSUR p2261 was provided by the Institut hospitalo-universitaire Méditerranée Infection, Marseille, France. Akkp2261 was grown on 5% sheep blood enriched Columbia agar (COS) plates in an anaerobic atmosphere created using 3 anaerobic generators (BioMerieux) at 37 °C for at least 72 hours. Identification of the bacterium was performed using a Matrix-Assisted Laser Desorption/Ionization Time of Flight (MALDI-TOF) mass spectrometer (Microflex LT analyzer, Bruker Daltonics). Colonization of ATB pre-treated mice was performed by oral gavage with 100 µl of suspension containing 1×10^8 bacteria obtained from a suspensions of 1×10^9 CFU/ml using a fluorescence spectrophotometer (Eppendorf) at an optical density of 600 nm in PBS. Five bacterial gavages were performed for each mouse: the first 24 hours before the first injection of anti-PD-1 monoclonal antibodies and, subsequently, four times on the same day of ICI.

Mouse fecal DNA extraction and microbiota characterization. Feces were collected from each mouse and group for metagenomics between 7 and 14 days after start of immunotherapy. Samples were stored at −80 °C until processing. Preparation and sequencing of mouse fecal samples was performed at IHU Méditerranée Infection, Marseille, France. Briefly, DNA was extracted using two protocols. The first protocol consisted of physical and chemical lysis using glass powder and proteinase K, respectively, then processing using the Macherey-Nagel DNA Tissue extraction kit (Duren). The second protocol was identical to the first protocol, with the addition of glycoprotein lysis and deglycosylation steps. The resulting DNA was sequenced, targeting the V3–V4 regions of the 16S rRNA gene. Raw FASTQ files were analyzed with Mothur pipeline v.1.39.5 for quality check and filtering (sequencing errors, chimerae) on a Workstation DELL T7910. Raw reads were filtered and clustered into Operational Taxonomic Units (OTUs), followed by elimination of low-populated OTUs (until 5 reads) and by de novo OTU picking at 97% pair-wise identity using standardized parameters and SILVA rDNA Database v.1.19 for alignment. A prevalence threshold of ≥2.5% was implemented for statistical analyses on recognized OTUs, performed with Python v3.8.2. The most representative and abundant read within each OTU (as evidenced in the previous step with Mothur v.1.39.5) underwent a nucleotide blast using the National Center for Biotechnology Information (NCBI) Blast software (ncbi-blast-2.9.0) and the latest NCBI 16S Microbial Database (ftp://ftp.ncbi.nlm.nih.gov/blast/db/). A matrix of bacterial relative abundances was built at each taxon level (phylum, class, order, family, genus, species) for subsequent multivariate statistical analyses.

Statistical analyses. In humans, data matrices were firstly normalized then standardized using QuantileTransformer and StandardScaler methods from Sci-Kit learn package v0.20.3. Normalization using the output_distribution = 'normal' option transforms each variable to a strictly Gaussian-shaped distribution, while the standardization results in each normalized variable having a mean of zero and variance of one. These two steps of normalization followed by standardization ensure the proper comparison of variables with different dynamic ranges, such as bacterial relative abundances. For microbiota analysis, measurements of α diversity (within-sample diversity) such as Richness and Shannon index, were calculated at species level using the SciKit-learn package v.0.4.1. Exploratory analysis of β-diversity (between-sample diversity) was calculated using the Bray–Curtis measure of dissimilarity and represented in Principal Coordinate Analyses (PCoA), along with methods to compare groups of multivariate sample units (analysis of similarities (ANOSIM), permutational multivariate analysis of variance (PERMANOVA)) to assess significance in data points clustering. ANOSIM and PERMANOVA were automatically calculated after 999 permutations, as implemented in SciKit-learn package v0.4.1. We implemented partial least square discriminant analysis (PLS-DA) and the subsequent variable importance plot (VIP) as a supervised analysis wherein the VIP values (order of magnitude) are used to identify the most discriminant bacterial species. All the analyses were performed within a Python v3.8.2 environment. Univariate differential abundance analysis was performed via linear discriminant analysis of effect size (LEfSe)[61]. We added further support of differentially abundant species using two different multivariate differential abundance methods, ANCOM-BC[62] and MaAsLin2[63], which included covariates such as age, sex, BMI, cohort, and sequencing batch. France's Data Protection Article 8 legislation (Commission Nationale Informatique et Libertés) prohibits the analysis of the racial and ethnic origins. Raw sequencing counts were estimated from species-level MetaPhlAn 3 relative abundances by multiplying these values by the total number of reads for each sample and these were used in ANCOM-BC (v.1.0.1) with default parameters, a library size cutoff of 500 reads and no structural zero detection. Masslin2 (v.1.4.0) was run using Logit-transformed relative abundances that were normalized with total-sum-scaling (TSS) and using the variable of interest as a fixed effect.

Survival curves were estimated using the Kaplan–Meier method and compared with the log-rank test (Mantel–Cox method) in a univariate analysis. Multivariate analyses were performed using Cox regression models to determine HRs and 95% confidence intervals (CIs) for OS, adjusting for other clinicopathologic features. The proportionality hazard assumption was checked testing the trend of the Schoenfeld residuals with the cox.zph R function. When the test was statistically significant for a variable, its interaction with time was introduced in the model and tested using the tt (time transformation) function with different functional forms (linear, exponential, logarithmic, and penalized spline). The optimal cutoff for each bacterial species to define different prognosis groups was obtained with grid search algorithm based on the multivariate Cox model to take into account the potential confounding factors (such as age and sex). The grid was defined for each species by the percentiles of the distribution of the non-zero prevalence values. The cutoff corresponding to the model with the better Akaike information criterion (AIC, lower is better) was selected as the optimal cutoff.

All tests were two-sided and statistical significance was set at $P < 0.05$. Statistical analyses were conducted using the GraphPad Prism 7 and R software (http://www.R-project.org/).

In mice, all tumor growth curves were analyzed using software developed in Kroemer's laboratory: https://kroemerlab.shinyapps.io/TumGrowth/. Between-group comparisons of mice and global comparisons were performed using a Kruskall–Wallis test and post-hoc multiple comparisons using Dunn's test. Finally, natural tumor growth data deriving from mice experiments (6 mice per experiment) were averaged for each timepoint (T0 to T8), then longitudinally normalized on the first timepoint, in order to have a common starting value of 1. All averaged and normalized tumor values were then expressed with fold ratios (FR; Extended Data Fig. 6E), and underwent base 2 logaritmization in order to enhance augmentation (red) or diminution (blue) of the tumor growth. A hierarchical clusterization analysis based on Bray–Curtis distance was implemented on longitudinal FR data in order to define a branch of responder to Akkp2261 (Extended Data Fig. 6E, green cluster) or a group of non-responder to Akkp2261 (Extended Data Fig. 6E, red cluster). A reported *P* values (i.e., $*P \leq .05$, $**P \leq .01$, $***P \leq .001$) underwent Benjamini–Hochberg two-stage false-discovery rate (FDR) at 10%.

Data availability

The data generated or analyzed during this study are included within the paper, its Supplementary Information files and public repositories. Detailed information on the cohort is available in Supplementary Table 8 raw metagenomic sequences are available in the SRA under the Bioproject accession PRJNA751792 (https://www.ncbi.nlm.nih.gov/bioproject/PRJNA751792) and PRJNA782662 (https://www.ncbi.nlm.nih.gov/bioproject/PRJNA782662), and raw RNA sequencing are available in the SRA under accession the NCBI accession GSE182328 (https://www.ncbi.nlm.nih.gov/geo/query/acc.cgi?acc=GSE182328). All BioSample (PATIENTS_Metadata.csv) are also provided as supplementary information. Source data are provided with this paper.

Code availability

No unique software or computational code was created for this study. Code detailing implementation of established tools/pipelines are described in details in the Method section and available upon request to the corresponding author.

References

55. Eisenhauer, E. A. et al. New response evaluation criteria in solid tumours: revised RECIST guideline (version 1.1). *Eur. J. Cancer* **45**, 228–247 (2009).
56. Li, J. et al. An integrated catalog of reference genes in the human gut microbiome. *Nat. Biotechnol.* **32**, 834–841 (2014).
57. Nielsen, H. B. et al. Identification and assembly of genomes and genetic elements in complex metagenomic samples without using reference genomes. *Nat. Biotechnol.* **32**, 822–828 (2014).
58. Beghini, F. et al. Integrating taxonomic, functional, and strain-level profiling of diverse microbial communities with bioBakery 3. *Elife* **10**, e65088 (2021).
59. Fumet, J.-D. et al. Prognostic and predictive role of CD8 and PD-L1 determination in lung tumor tissue of patients under anti-PD-1 therapy. *Br. J. Cancer* **119**, 950–960 (2018).
60. Bray, N. L., Pimentel, H., Melsted, P. & Pachter, L. Near-optimal probabilistic RNA-seq quantification. *Nat. Biotechnol.* **34**, 525–527 (2016).
61. Segata, N. et al. Metagenomic biomarker discovery and explanation. *Genome Biol.* **12**, R60 (2011).
62. Lin, H. & Peddada, S. D. Analysis of compositions of microbiomes with bias correction. *Nat. Commun.* **11**, 3514 (2020).
63. Mallick, R. et al. Subduction initiation and the rise of the Shillong Plateau. *Earth Planet. Sci. Lett.* **543**, 116351 (2020).

Acknowledgements

L. Z. and B. B. were funded by the RHU Torino Lumière (ANR-16-RHUS-0008), while L. Z. was supported by H2020 ONCOBIOME and ANR, French–German Ileobiome, 19-CE15-0029-01. L. Z. and G. K. received a donation from Seerave Foundation. L. Z., L. D., and E. D. were supported by the SIRIC Stratified Oncology Cell DNA Repair and Tumor Immune Elimination (SOCRATE). L. D. and L. Z. were supported by SIGN'IT 2020 ARC foundation. This work was also supported by the Prism project funded by the Agence Nationale de la Recherche under grant number ANR-18-IBHU-0002.
L. Z. and G. K. were supported by the Ligue contre le Cancer (équipe labelisée); ANR Projets blancs; ANR under the frame of E-Rare-2, the ERA-Net for Research on Rare Diseases; Association Pour La Recherche Sur Le Cancer (ARC); Bristol-Myers Squibb (BMS) (International Immuno-Oncology Network), Cancéropôle Ile-de-France; Chancellerie des Universités de Paris (Legs Poix), Fondation pour la Recherche Médicale (FRM); a donation by Elior; the European Commission (ArtForce); the European Research Council (ERC); Fondation Carrefour; Institut National du Cancer (INCa); Inserm (HTE); Institut Universitaire de France; LeDucq Foundation; the LabEx Immuno-Oncology; FHU CARE, Dassault, and Badinter Philantropia, and the Paris Alliance of Cancer Research Institutes (PACRI). B. R. is supported by the Canadian Institutes of Health Research (CIHR), Institut du cancer de Montreal and the Prefontaine family. A. C. is supported by the CPRIT Research Training Program (RP170067). N. S. was supported by the European Research Council (ERC-STG project MetaPG-716575); MIUR 'Futuro in Ricerca' (grant No. RBFR13EWWI_001); the European H2020 program (ONCOBIOME-825410 project and MASTER-818368 project); the National Cancer Institute of the National Institutes of Health (1U01CA230551); by the Premio Internazionale Lombardia e Ricerca 2019 to G. K. A. M. has been or is currently an investigator in clinical trials sponsored by BMS, MSD, GlaxoSmithKline (GSK)/Tesaro, Janssen, Roche/Genentech, Pfizer, AstraZeneca, Amgen. A. M. has been or is currently a member of Clinical Trial Scientific Steering Committee for AstraZeneca and GSK. A. M. has been or is currently a member of the scientific advisory board of the following companies: Merck Serono, Novartis, BMS, Symphogen, Amgen, Tesaro/GSK, Pfizer, AstraZeneca/Medimmune, Servier, and Sanofi. A. M. has provided scientific and medical consulting to the following companies: Roche, Sanofi. A. M. is a member of the data safety and monitoring board for trial NCT02423863 (TLR3 agonist; Oncovir). A. M. has received research funding and/or drug supply for preclinical and clinical research projects from: BMS, Boehringer Ingelheim, Idera, MSD, Fondation MSD Avenir, and SIRIC (INCa-DGOS-Inserm_12551).

Author contributions

L. Z., L. D., B. R., and B. B. conceived the study. L. D. and B. R. orchestrated the ONCOBIOTICS study. B. B. coordinated the clinical inclusions. L. D., G. Z., S. F., J. M., C. A.-V., D. M.-S., F. Goldwasser, A. S., H. P., F. Ghiringhelli, F. B., D. P., S. M., N. B., B. B., and J. C. S. enrolled patients and managed patient stool collection. L. D., C. A. C. S., M. B., S. T., and B. R. coordinated the ONCOBIOTICS network for stool traceability and data collection and management. F. B.-D. recovered the Tumor Mutational Burden. F. C., A. B., and N. S. worked on the new markers for Akk in MetaPhlAn 3. R. B. and S. C. worked on RNA-seq. A. M. T., V. I., and N. S. interpreted the MG analyses and performed independent statistical analyses. C. R. O. Absilon planned the data management and kept the electronic files. D. D. double checked the statistical analyses. L. D., A. D., B. R., and M. M. designed the figures. R. D. and L. D. managed mice experiments. E. L. C., L. A., N. P., N. G., H. R., managed the sequencing of stool samples G. K. participated in data interpretation and edited the paper. All authors participated in paper editing.

Competing interests

L. Z. received research contract from Kaleido and Innovate Pharma and Pilege. L. D. has consulted for and had an advisory role for BMS and Sanofi and was supported by Philantropia Fondation Gustave Roussy. G. Z. received a research grant from Fondation Roche, received fees from Roche, MSD, BMS, and Astra-Zeneca, and is consultant for Da Volterra and Inventiva. L.Z and R.D. are the scientific cofounders of Everimmune. E. D. reports grants and personal fees from Roche Genentech, grants from Boehringer, grants from AstraZeneca, grants and personal fees from Merck Serono, grants from BMS, and grants from MSD. P. D. has had consulting and advisory roles for AstraZeneca, BMS, Boehringer Ingelheim, Celgene, Daiichi Sankyo, Eli Lilly, Merck, Novartis, Pfizer, prIME Oncology, Peer CME, Roche, and Samsung, as well as honoraria from AstraZeneca, BMS, Boehringer Ingelheim, Celgene, Eli Lilly, Merck, Novartis, Pfizer, prIME Oncology, Peer CME, Roche, and Samsung. P. D. ran clinical trials as principal or co-investigator for AstraZeneca, BMS, Boehringer Ingelheim, Eli Lilly, Merck, Novartis, Pfizer, Roche, Medimmun, Sanofi-Aventis, Taiho Pharma, Novocure, and Daiichi Sankyo, and has received travel or accommodation expenses from AstraZeneca, Roche, Novartis, prIME Oncology, and Pfizer. F. G. received honoraria from Amgen, Sanofi, Merk Serono, MSD, BMS, and AstraZeneca, had a consultancy or advisory role for Roche and Enterome, and received direct research fundings from Roche, Enterome, AstraZeneca, and Servier and traveling support from Servier, Amgen, and Roche. J. C. S. in the last 2 years has received consultancy fees from Relay Therapeutics and Gritstone and holds shares of Hookipa, Gritstone, AstraZeneca, and Daiichi Sankyo, and was a full time employee for AstraZeneca in 2017–2019. The remaining authors declare no competing interests.

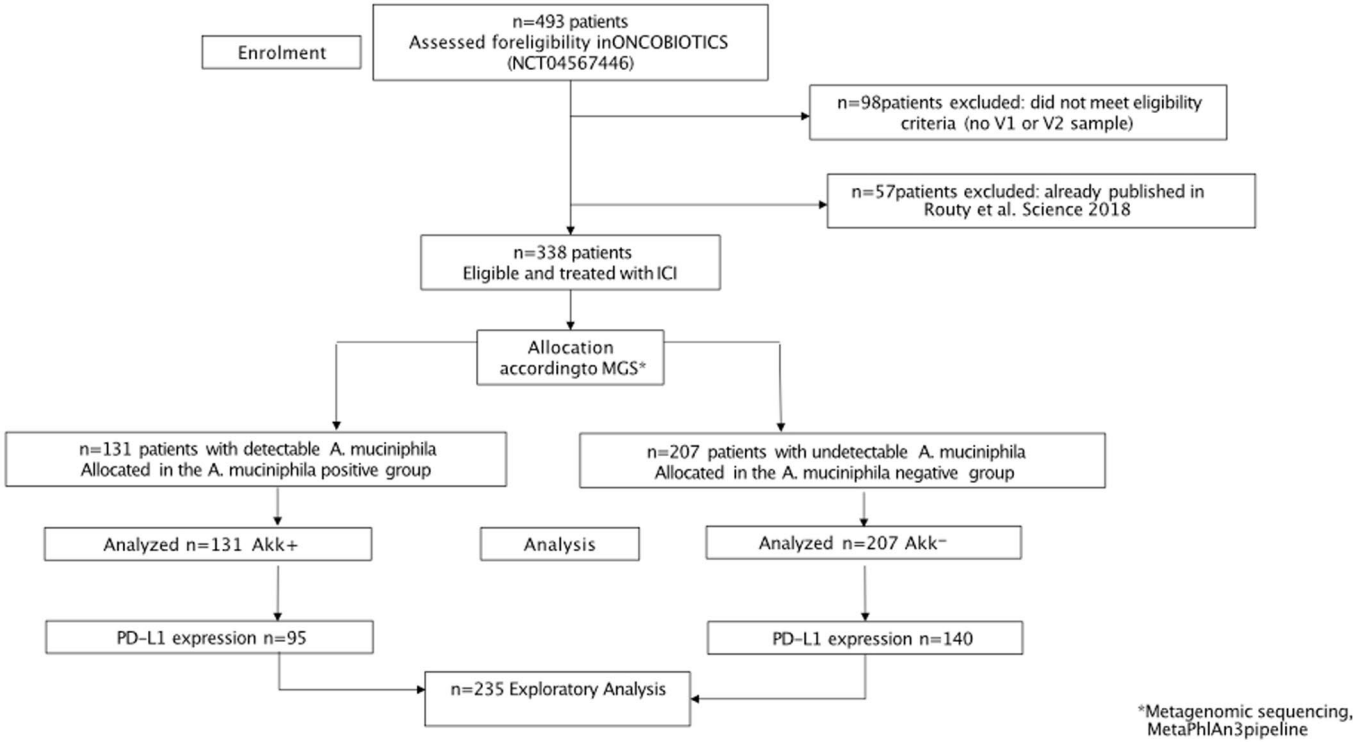

Extended Data Fig. 1 | Consort diagram describing the stool collection in the whole NSCLC ONCOBIOTICS cohort. Consortium diagram for patients enrollment in the ONCOBIOTICS study (n=493) according to stool availability, presence of *Akkermansia muciniphila (Akk)*, and tumor PD-L1 expression levels. V1; baseline fecal sample. V2; before the second injection of the immune checkpoint inhibitor; MGS: Metagenomic Sequencing. Akk^{+}: detection of *Akk;* Akk^{-}: no detection of *Akk* by shotgun metagaenomics sequencing (MGS) analysis at diagnosis.

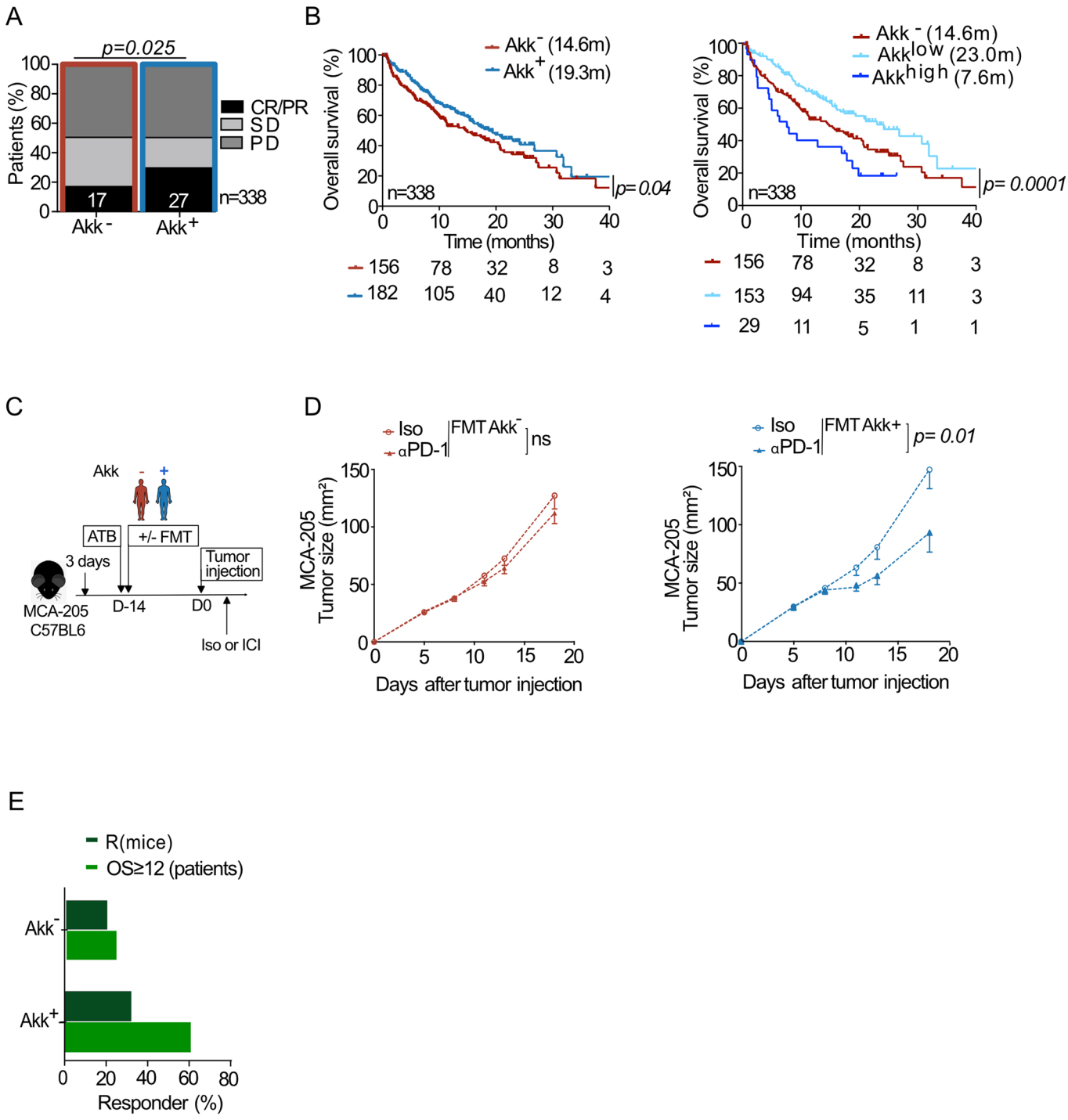

Extended Data Fig. 2 | MetaOMineR-based analysis of the association between stool *A. muciniphila (Akk)* and clinical benefit to ICI in patients. A-B. Correlations between stool prevalence of *Akk* (MetaOMineR pipeline) and ORR **(A)** or OS **(B)** in 1+2L NSCLC patients (N=338, **A-B**) based on MGS identification of Akk in the MetaOMineR algorithm (INRAE). Chi-square test (**A**) and Cox regression analysis for median overall survival (OS) depicted in Kaplan Meier curves according to detectable or undetectable *Akk* (Akk^+ or Akk) analyzed in 2 groups (**B**, left panel) or segregated in 3 groups (Akk^-, Akk^{low} and Akk^{high}) (**B**, right panel). Chi-square test *P*-values are two-sided, with no adjustments made for multiple comparisons (A). The Akk status was compared using the stratified log-rank test. *P*-values are one-sided with no adjustment (B). **C**. Experimental setting of avatar mice. FMT of NSCLC patients (Supplementary Table S3) segregated according to the presence or absence of *Akk* into MCA-205 tumor bearing C57BL/6 mice. Treatments are indicated by arrows (ATB, FMT, anti-PD-1 (ICI) mAbs, or isotype control mAbs (Iso)). **D**. MCA-205 tumor growth kinetics in each group of FMT according to the prevalence of *Akk*. in isotype Ctl *versus* anti-PD-1 mAbs treated mice. Data are presented as mean values +/-SEM of tumor sizes within 6 animals/group. Concatenation of at least n=8 experiments (using a different stool of NSCLC patient) containing 6 mice/group. Tumor sizes according to FMT Akk^- (**D**, left panel) versus Akk+ (**D**, right panel) are depicted, each dot representing one mouse. Statistics were mixed-effect modeling with specific software ((https://kroemerlab.shinyapps.io/TumGrowth/) for longitudinal tumor growth analysis. *P*-value are indicated. **E**. Percentages of responding mice (tumor reduction of>25 % compared with means of controls in the anti-PD-1 mAbs -treated group) and patients (ORR) in each category of stools used for FMT (derived from patients in Supplementary Table S3). CR; complete response. PR; partial response, SD; stable disease, PD; progressive disease.

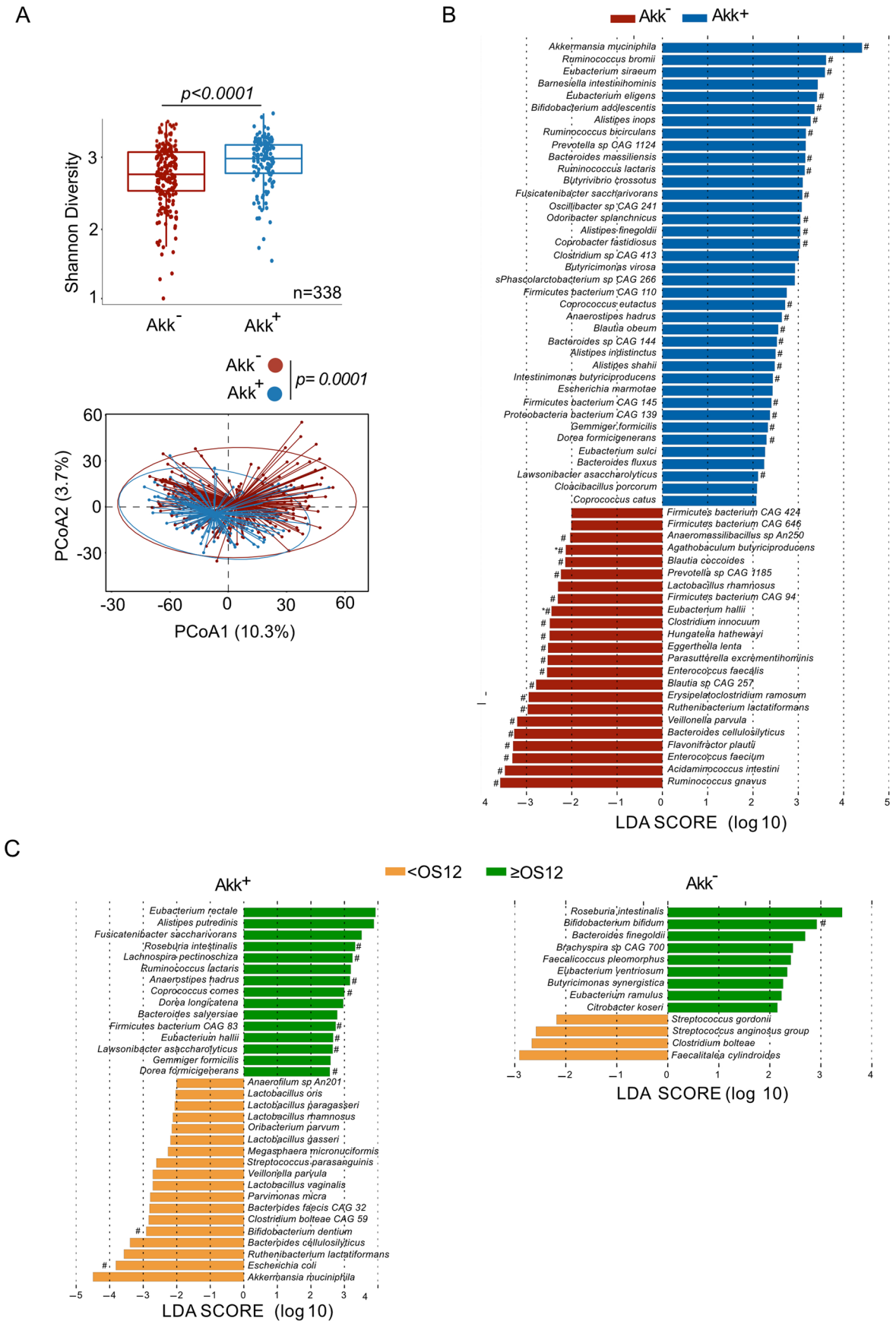

Extended Data Fig. 3 | See next page for caption.

Extended Data Fig. 3 | Metagenomic species characterizing *Akk*$^{+}$ stools and patient survival. Shannon diversity index representing stool alpha diversity in Akk^{+} and Akk^{-} groups of fecal specimens (N=338) (**A**, upper panel). Beta-diversity measured by Bray-Curtis Index represented by Principal Coordinates analysis (PCoA) between Akk^{+} *versus* Akk^{-} groups in the whole cohort of 1+2L (**A**, lower panel). *p*-values were calculated using PERMANOVA with 999 permutations. The lower and the upper hinges of boxplots corresponds to the 25th and 75th percentiles, respectively. The midline is the median. The upper and lower whiskers extend from the hinges to the largest (or smallest) value no further than ×1.5 interquartile range from the hinge, defined as the distance between the 25th and 75th percentiles. *P*-values were calculated testing the null hypothesis and using a two-sided test. Exact *p*-value: 3.84573e-05. **B-C**. Differential abundance of metagenomic species measured by linear discriminant analysis of effect size (LEfSe) according to the presence of *A. muciniphila (Akk)* **(B)** and the OS at 12 months **(C)** within Akk+ group (**C**, left panel) and Akk- group (**C**, right panel). LDA; Linear discriminant analysis. OS: overall survival. *P*-values were calculated using a two-sided nonparametric factorial Kruskal-Wallis (KW) sum-rank test. # Multivariate analysis (ANCOM-BC/ Maaslin2) with a false discovery rate (FDR) adjusted *p*-value <0.2.

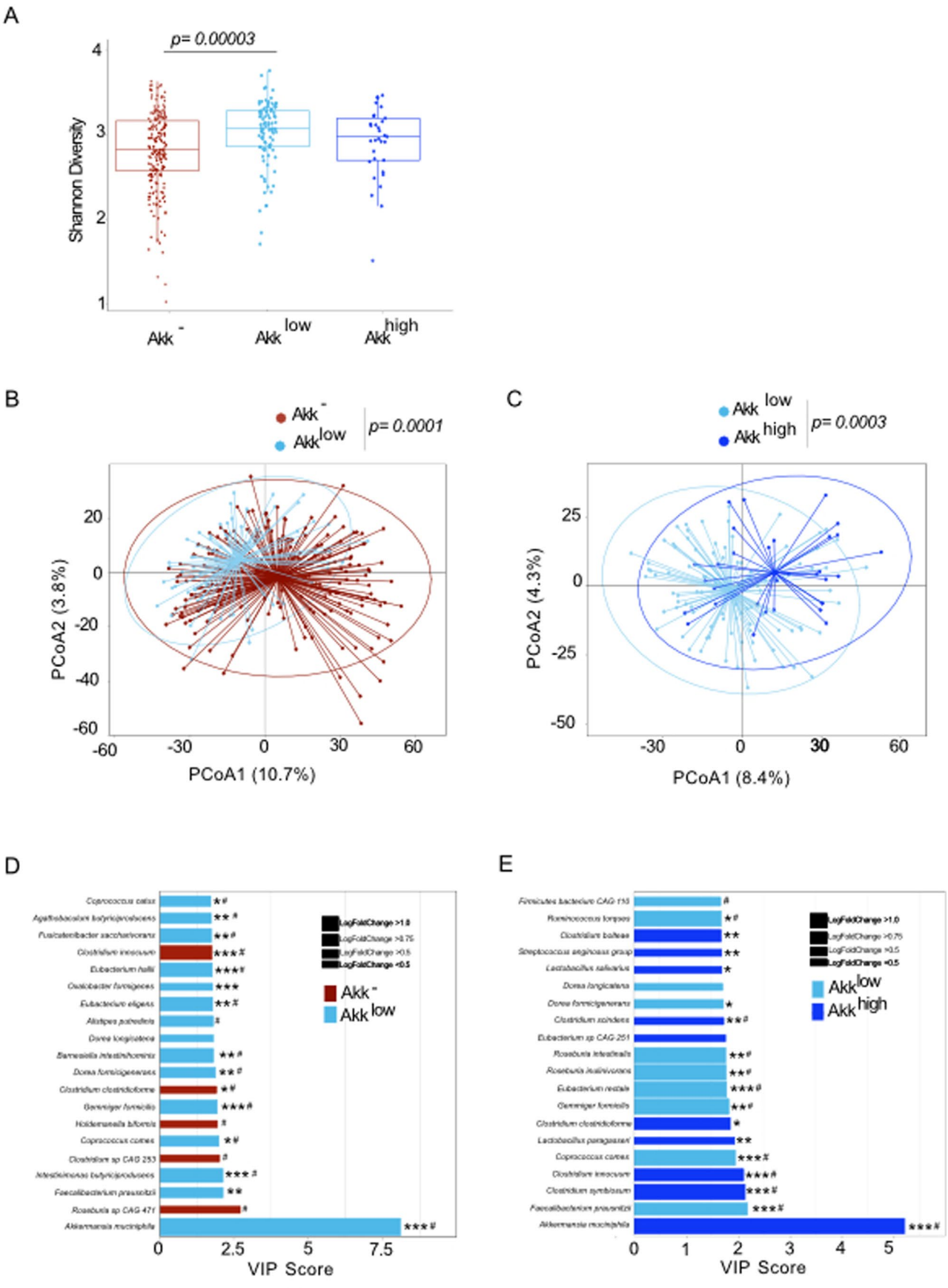

Extended Data Fig. 4 | See next page for caption.

Extended Data Fig. 4 | Compositional taxonomic differences in stools of NSCLC patients segregated according to Akk relative abundance. A. Alpha diversity according to *Akk* relative abundance segregated in 3 groups Akk^{-}: undetectable *Akk*, Akk^{low}: *A. muciniphila* relative abundance between 0.035-4.799% (<77th percentile of positive samples), and Akk^{high}: 4.799% (> 77th percentile) (N=338). The lower and upper hinges of boxplots correspond to the 25th and 75th percentiles, respectively. The midline is the median. The upper and lower whiskers extend from the hinges to the largest (or smallest) value no further than ×1.5 interquartile range from the hinge, defined as the distance between the 25th and 75th percentiles. *P*-values were calculated using a two-sided nonparametric Wilcoxon sum-rank test. **B-C**. Beta-diversity using PCoA between Akk^{-} and Akk^{low} (**B**) and between Akk^{low} and Akk^{high} (**C**) *p*-values were calculated using PERMANOVA with 999 permutations. The PERMANOVA test compares groups of objects and tests the null hypothesis that the centroids and dispersion of the groups are equivalent. The *P*-value is calculated by comparing the actual F test to that gained from (in this case 999) random permutations of the objects between the groups. If p <0.05, the null hypothesis is disregarded and we conclude that the centroids and dispersion between the groups are not equivalent. **D-E**. Variable importance plot (VIP) discriminant analysis of taxonomic stool composition according to Akk relative abundance, between Akk^{-} versus Akk^{low} (**D**) and Akk^{low} versus Akk^{high} (**E**). Differences in bacterial prevalence and abundance in fold ratios are indicated in these VIP plots. VIP: Variable importance plot. * *p* <0.05,** *p* <0.01, *** *p* <0.001. *P*-values were calculated using a two-sided nonparametric Wilcoxon sum-rank test. # Multivariate analysis (ANCOM-BC/Maaslin2) with a false discovery rate (FDR) adjusted *p*-value <0.2.

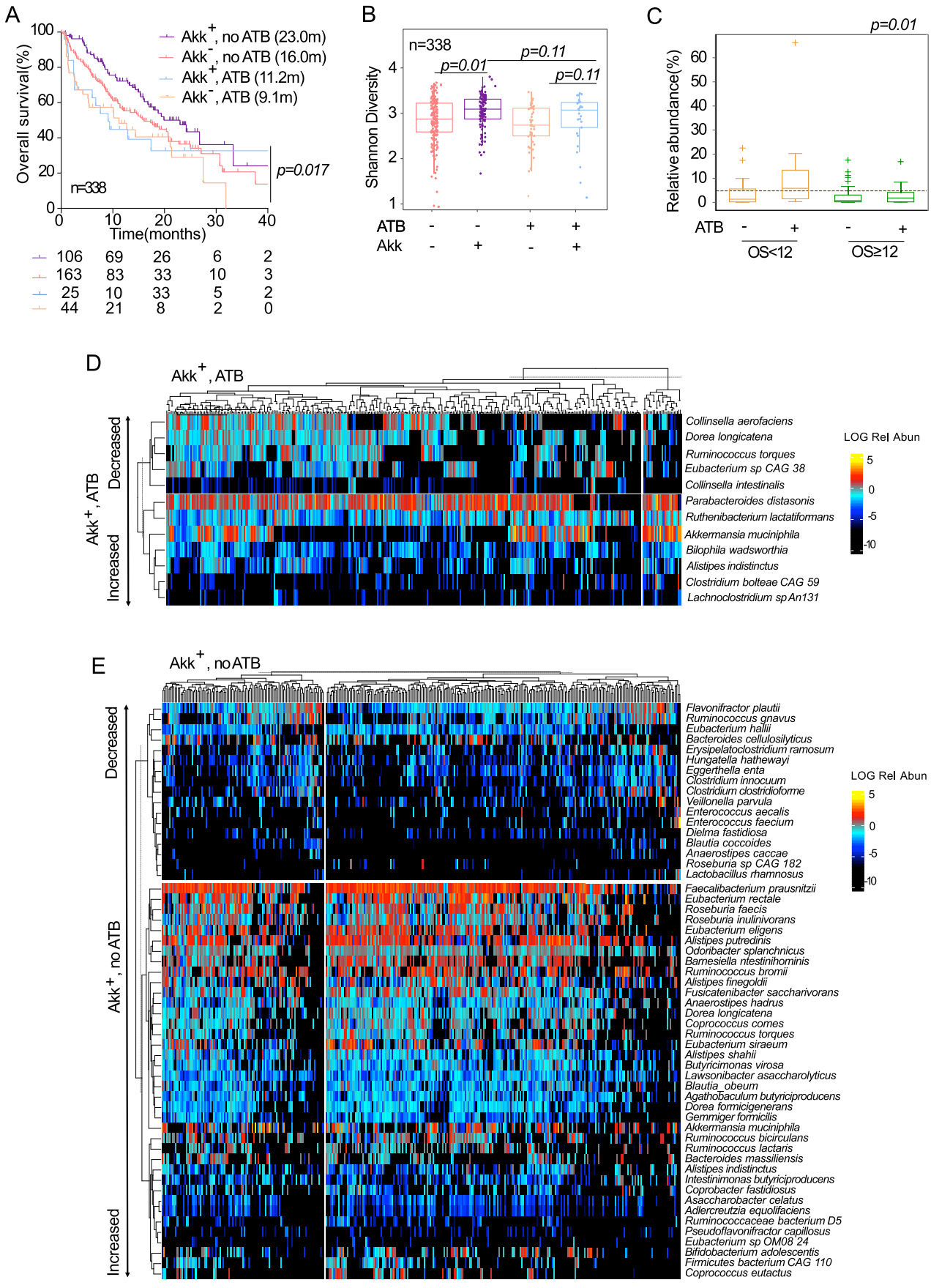

Extended Data Fig. 5 | See next page for caption.

Extended Data Fig. 5 | Interaction between ATB and *A.muciniphila* on survival and microbiome composition. A. Kaplan-Meier curve and Cox regression analysis of overall survival in the n=338 patients according to detectable *versus* undetectable *Akk* (Akk^+ and Akk^-) and ATB use (noATB: no exposure to ATB, ATB: antibiotics exposure within 2 months prior to ICI initiation). The Akk status and ATB use were compared using the stratified log-rank test. *P*-values are one-sided with no adjustment. **B**. Shannon diversity index representing stool alpha diversity in Akk^+ and Akk^- groups of fecal specimen from patients exposed or not to ATB (N=338). The lower and upper hinges of boxplots correspond to the 25th and 75th percentiles, respectively. The midline is the median. The upper and lower whiskers extend from the hinges to the largest (or smallest) value no further than ×1.5 interquartile range from the hinge, defined as the distance between the 25th and 75th percentiles. *P*-values were calculated using a two-sided nonparametric Wilcoxon sum-rank test. **C**. Box Plots representing the relative abundance (mean+/-SEM) of *Akk* according to overall survival at 12 months and exposure or not to ATB in n=338 patients. The lower and upper hinges of boxplots correspond to the 25th and 75th percentiles, respectively. The midline is the median. The upper and lower whiskers extend from the hinges to the largest (or smallest) value no further than ×1.5 interquartile range from the hinge, defined as the distance between the 25th and 75th percentiles. The test used was Kruskal-Wallis, two-sided, 5% level of significance. No adjustments were made for multiple comparisons. **D**. Heatmap showing differentially abundant species identified in stools with detectable *Akk* (Akk^+) in patients exposed to (D) or not exposed to (E) ATB within 2 months prior to ICI initiation. Species were identified using a non-parametric Kruskall-Wallis test comparing 4 groups made up of 2 variables: *Akkermansia muciniphila* presence/absence and antibiotic use. The figure shows species' abundances across samples whose False Discovery Rate (FDR) was <0.2 in the KW test and whose Wilcoxon Rank Sum Test *p*-value was <0.05 when comparing the highlighted group to the rest.

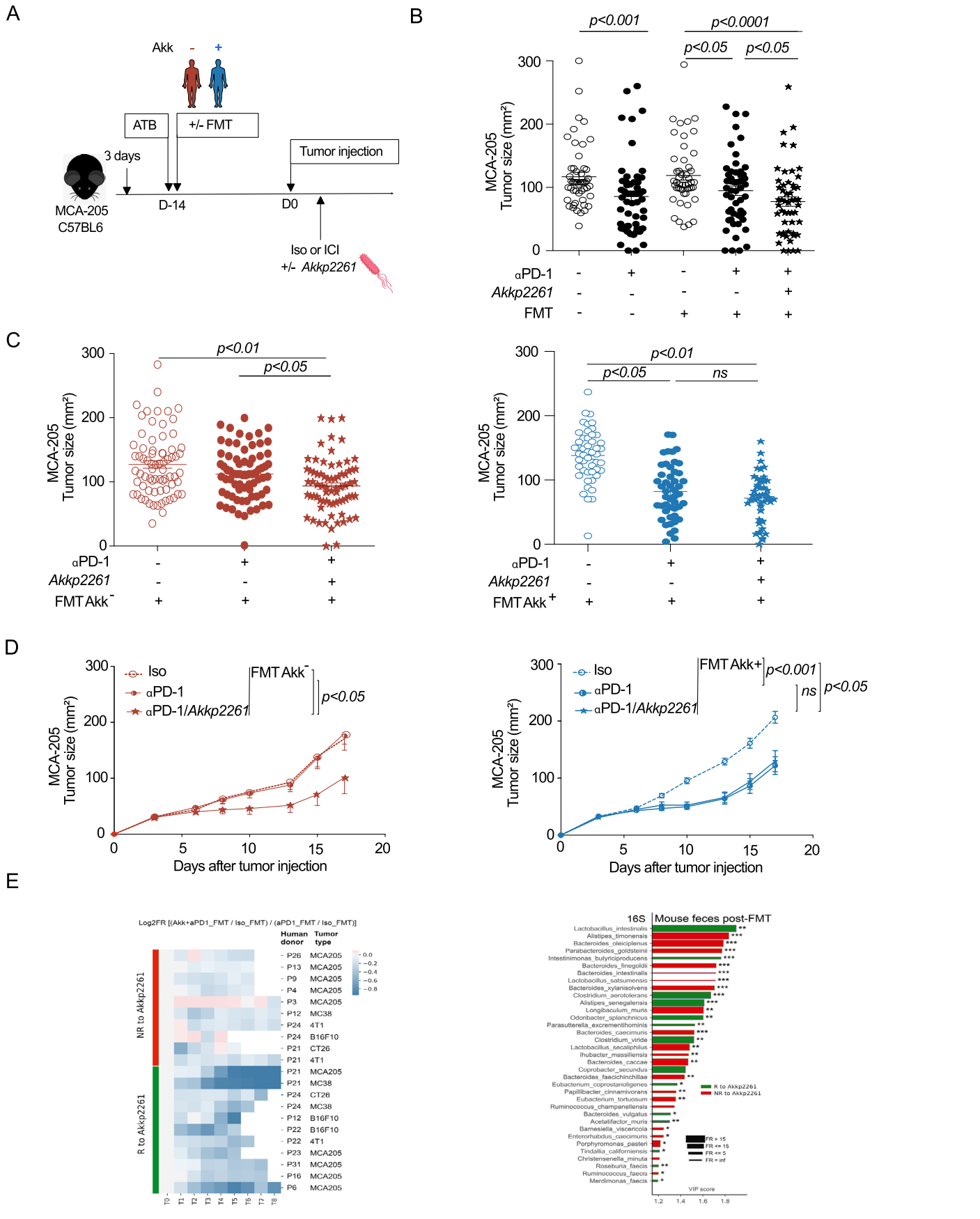

Extended Data Fig. 6 | See next page for caption.

Extended Data Fig. 6 | *Akkp2261* modulated the murine microbiome composition, rescuing responsiveness to PD-1 blockade. A. Experimental setting. After 3 days of ATB, FMT was performed in mice by oral gavage using patient stools classified according to *Akk* (Akk^+ and Akk^-). 14 days later, MCA-205 tumors were i.d inoculated, and mice were treated with anti-PD-1 or iso-control mAbs 4 times every 3 days concomitantly with oral supplementation of *Akkp2261* four times every 3 days. **B-D**. Mean MCA-205 tumor sizes+/-SEM are depicted at day 12 after 4 therapeutic injections of anti-PD-1 mAbs, in each FMT groups (Akk^+ and Akk^-) supplemented or not with *Akkp2261* as well as in animals reared in SPF conditions (FMT-). Concatenation of>25 experiments using n=53 mice in Iso group, n=51 in Iso FMT+ group, n=56 in anti-PD-1 and anti-PD-1 FMT+ groups. Each experiment comprising 6 mice/group and was performed at least 2 times for each FMT (Supplementary Table S6) **(B)**. Tumor sizes according to FMT Akk^- **(C left**, n=72/group; **C right**, n=49 in Iso group and n=48 in other groups) *versus* Akk^+ **(D left**, n=6/group**, D right**, n=12 in Iso and anti-PD-1 groups, n=14 in anti-PD-1 with *Akkp2261***)** are depicted, each dot representing one mouse. Statistics were mixed-effect modeling with specific software ((https://kroemerlab.shinyapps.io/TumGrowth/) for longitudinal tumor growth analysis **(D)** and Mann–Whitney U-test **(B-C)** to compare two independent groups (after Kruskal–Wallis test was implemented using Dunn's test for multiple groups). ns=not significant. **E**. Clustermap of ratios of *Akkp2261*-related tumor reduction at day 12-15 following PD-1 mAbs in FMT normalized onto ratios obtained in SPF mice. The relative tumor size reduction follows a blue color code (the darker the greater; R, Responders)). 29 FMT were performed according to A. N=29-30 mice/group in total. Each experiment contained 6 mice/group and was performed 2-3 times for each tumor model (**E**, left panel). 16S rRNA sequencing of gene amplicons of stools harvested in recipient avatar tumor bearers at day 12 post-4 injections of anti-PD-1 Abs and 4 oral gavages with *Akkp2261* divided into green (R) and red (NR) groups. VIP plot repartition of discriminant metagenomic species segregating groups of mice that responded to oral *Akkp2261* (R, green bars) or not (NR, red bars). (E, right panel). Asterisks represent significant Mann-Whitney U test without FDR at 10%. * p <0.05, ** p <0.01, *** p <0.001. P-values were calculated using a two-sided nonparametric Wilcoxon sum-rank test. Adjustments for multiple comparisons were not made.